



Immiscible Viscous Fingering: The Effects of Wettability/Capillarity and Scaling

A. Beteta¹ · K. S. Sorbie^{1,2} · A. Skauge^{1,2} · T. Skauge²

Received: 7 April 2023 / Accepted: 29 October 2023 / Published online: 22 November 2023
© The Author(s) 2023

Abstract

Realistic immiscible viscous fingering, showing all of the complex finger structure observed in experiments, has proven to be very difficult to model using direct numerical simulation based on the two-phase flow equations in porous media. Recently, a method was proposed by the authors to solve the viscous-dominated immiscible fingering problem numerically. This method gave realistic complex immiscible fingering patterns and showed very good agreement with a set of viscous unstable 2D water → oil displacement experiments. In addition, the method also gave a very good prediction of the response of the system to tertiary polymer injection. In this paper, we extend our previous work by considering the effect of wettability/capillarity on immiscible viscous fingering, e.g. in a water → oil displacements where viscosity ratio (μ_o/μ_w) $\gg 1$. We identify particular wetting states with the form of the corresponding capillary pressure used to simulate that system. It has long been known that the broad effect of capillarity is to act like a nonlinear diffusion term in the two-phase flow equations, denoted here as $D(S_w)$. Therefore, the addition of capillary pressure, $P_c(S_w)$, into the equations acts as a damping or stabilisation term on viscous fingering, where it is the *derivative* of this quantity that is important, i.e. $D(S_w) \sim (dP_c(S_w)/dS_w)$. If this capillary effect is sufficiently large, then we expect that the viscous fingering to be completely damped, and linear stability theory has supported this view. However, no convincing numerical simulations have been presented showing this effect clearly for systems of different wettability, due to the problem of simulating realistic immiscible fingering in the first place (i.e. for the viscous-dominated case where $P_c = 0$). Since we already have a good method for numerically generating complex realistic immiscible fingering for the $P_c = 0$ case, we are able for the first time to present a study examining both the viscous-dominated limit and the gradual change in the viscous/capillary force balance. This force balance also depends on the physical size of the system as well as on the length scale of the capillary damping. To address these issues, scaling theory is applied, using the classical approach of Rapport (1955), to study this scaling in a systematic manner. In this paper, we show that the effect of wettability/capillarity on immiscible viscous fingering is somewhat more complex and interesting than the (broadly correct) qualitative description above. From a “lab-scale” base case 2D water → oil displacement showing clear immiscible viscous fingering which we have already matched very well using our numerical method, we examine the effects of introducing either a water wet (WW) or an oil wet (OW) capillary pressure, of different “magnitudes”. The

characteristics of these two cases (WW and OW) are important in how the value of corresponding $D(S_w)$ functions, relate to the (Buckley–Leverett) shock front saturation, S_{wf} , of the viscous-dominated ($P_c = 0$) case. By analysing this, and carrying out some confirming calculations, we show clearly why we expect to see much clearer immiscible fingering at the lab scale in oil wet rather than in water wet systems. Indeed, we demonstrate why it is very difficult to see immiscible fingering in WW lab systems. From this finding, one might conclude that since no fingering is observed for the WW lab-scale case, then none would be expected at the larger “field” scale. However, by invoking scaling theory—specifically the viscous/capillary scaling group, C_{VC1} , (and a corresponding “shape group”, C_{S1}), we demonstrate very clearly that, although the WW viscous fingers do not usually appear at the lab scale, they emerge very distinctly as we “inflate” the system in size in a systematic manner. In contrast, we demonstrate exactly why it is much more likely to observe viscous fingering for the OW (or weakly wetting) case at the lab scale. Finally, to confirm our analysis of the WW and OW immiscible fingering conclusions at the lab scale, we present two experiments in a lab-scale bead pack where $(\mu_o/\mu_w) = 100$; no fingering is seen in the WW case, whereas clear developed immiscible fingering is observed in the OW case.

Keywords Viscous fingering · Effect of wettability on viscous fingering · Effects of capillarity on viscous fingering · Scaling of capillary/viscous fingering · Effect of capillary pressure on viscous instability in porous media

1 Introduction and Literature Review

1.1 Viscous Fingering (VF) Literature

Instability is a central feature of flows in fluid mechanics, where the subject is closely related to the transition to turbulence (Drazin and Read 2004). Fluid instabilities in porous media do have some formal resemblance to the general characteristics of free fluids and can be analysed using some similar techniques such as stability analysis, although the specifics of instabilities in porous media are somewhat different (Drazin and Read 2004). A particular instability can be observed in porous media when a low viscosity fluid directly displaces a higher viscosity fluid, and this is usually referred to as viscous fingering. The two fluids may be fully miscible, partly miscible or immiscible, but in this work we will focus on the specific problem of *immiscible viscous fingering*. Examples of immiscible fingering in porous media can be seen when a gas, such as H_2 or CO_2 , displaces water in an aquifer (under certain conditions) or when water (viscosity, μ_w) displaces a high viscosity oil (μ_o). In the latter case, the severity of the viscous fingering depends on the viscosity ratio, (μ_o/μ_w) .

Since the initial founding work on this topic (Engleberts and Klinkenberg 1951; Hill 1952; Van Meurs and Van der Poel 1958; Saffman and Taylor 1958; Chuoke et al. 1959) a huge literature has appeared on viscous fingering which is reviewed in several publications (e.g. Homsy 1987; Calderon et al. 2007; Pinilla et al. 2021; Salmo et al. 2022). The last reference in this list reviews immiscible viscous fingering in some detail under the headings of (a) linear stability analysis of the initial finger growth; (b) direct numerical simulation of immiscible fingering; (c) experimental studies at the core/2D slab scale; (d) discrete and pore scale modelling of viscous fingering (Salmo et al. 2022). We focus here mainly of the

summary of areas (b) and (c) since this is the main topic of this paper; a brief summary is as follows:

(a) *Linear stability analysis of immiscible fingering* Linear stability analysis of two-phase immiscible fingering was originally proposed to analyse the early time growth of unstable modes by Chuoke et al. (1959). This has been extensively developed by many workers (Huang et al. 1984; Yortsos and Huang 1986; Alemán and Slattery 1988; Chikhliwala et al. 1988; Chikhliwala et al. 1988; Yortsos and Hickernell 1989; Yortsos 1990; Riaz and Tchelepi 2006a; Daripa and Pasa 2008). The broad objective is to determine if there are some longer wavelength modes of the perturbation which will grow over time leading to instability. The stabilising effect of capillary pressure is important in this respect and is of relevance to the work presented here, especially the work of Yortsos and Hickernell (1989) and Daripa and Pasa (2008).

(b) *Direct numerical simulation of immiscible fingering* Numerical simulation seeks to make direct comparison between continuum numerical modelling by some particular method, and experimental viscous fingering experiments (see below) for any viscosity ratios, (μ_o/μ_w) . The early success of Blunt et al. (1994) has not been significantly improved upon, by later publications using either more elaborate numerical methods (e.g. Riaz and Tchelepi 2006a, b; Erandi et al. 2015; Mostaghimi et al. 2016; Adam et al. 2017; Hamid and Muggeridge 2018; Kampitsis et al. 2019, 2020) or more conventional numerical approaches (Berg and Ott 2012; de Loubens et al. 2018; Bakharev et al. 2020; Chaudhuri and Vishnudas 2018). It is in this area that the current work is located, and follows some previous papers from the authors where direct numerical simulation *does* lead to very detailed fingers which agrees well with experiment (Sorbie et al. 2020; Salmo, et al. 2022; Beteta et al. 2022a).

(c) *Experimental results on immiscible fingering* Since the earliest work on immiscible viscous fingering appeared (Engleberts and Klinkenberg 1951; van Meurs and van der Poel 1958), almost no complete experimental studies have been published allowing direct numerical simulations to be tested. In this context, by “complete” we mean having the time lapsed finger patterns of the immiscible fingers, along with the oil recovery, watercut and pressure drop profiles (vs. pore volume injected, PV). The two exceptional bodies of work are as follows: (i) The collected experimental/modelling studies of Mohanty, Doorwar and colleagues in the USA (Doorwar and Mohanty 2011, 2014a, b, 2017; Doorwar and Ambastha 2020) who studied immiscible viscous fingering in a series of micromodel and core flooding experimental and modelling papers. The focus of this work was to develop models of the fingering for use in upscaled simulations of unstable displacement processes, following the “averaging tradition” of constructing “finger functions” (Koval 1963; Fayers 1988; Fayers and Newley 1988; Tardy and Pearson 2005). This is a particular approach to solving the “unresolvable finger” problem and leads to practical workflows for modelling these processes. However, in this paper, we focus more of direct numerical modelling of resolved fingering (Sorbie et al. 2020), and to validate this, we have used experimental results from the second significant literature body of immiscible fingering results as follows: (ii) The work over the last 12 or so years of Skauge and colleagues in Norway (Skauge et al. 2009, 2011, 2012, 2013, 2014; Skauge and Salmo 2015; Bondino et al. 2011; Fabbri et al. 2015, 2020; Salmo et al. 2017; de Loubens et al. 2018). Unstable waterfloods (and tertiary polymer floods) were performed on 2D slabs of Bentheimer sandstone, and the full data set of oil recovery, watercut and pressure drop profiles and in situ X-ray images of the finger patterns (all vs. PV injected) were reported. In our previous work, all of this data was used to test our simulation methodology (Sorbie et al. 2020) to model immiscible viscous fingering with oil/water viscosity ratios over the range, $(\mu_o/\mu_w) \sim 100\text{--}7000$ (Salmo

et al. 2022; Beteta et al. 2022a). The agreement between the experiment and direct simulations were all between very good and excellent.

The published body of experimental work on the specific study of *wettability* on viscous fingering is quite small. Worawutthichanyakul and Mohanty (2017) performed a series of core floods in oil wet rock cores. They observed that, in oil wet experiments, the breakthrough oil recovery decreases as the flow rate decreases, whereas in water wet systems it increases. Hence, a correlation previously developed for water wet cores did not apply to their results. They went on to develop a new correlation but with the intent of carrying on their long-standing programme of devising pseudo-relative permeabilities to describe and upscale the fingering process in large-scale simulations. Zhao and Mohanty (2019) noted that viscous fingering was more severe in strongly oil wet media than in weakly oil wet media or water wet media, and again found different correlations for each wetting system. Zhao (2020) gives a good review of the rather limited literature on the effects of wettability on immiscible viscous fingering.

(d) *Discrete and pore scale modelling* Our previous review briefly touched on the vast literature on pore scale model using the various (non-continuum) approaches such as lattice Boltzmann, network modelling, etc. (Salmo et al. 2022). However, since pore scale modelling has little direct bearing on the main topic of this paper, no more will be added here.

1.2 The Problem of Modelling Viscous Fingering by Direct Numerical Simulation

Various equivalent formulations of the macroscopic equations (coupled PDEs) describing two-phase flow in porous media are quite well known (Bear 1989; Peaceman 1977; Aziz and Settari 1979; Pinder and Gray 2008; Wu 2015), and these will be discussed below. Numerical methods have been applied to solve these equations and many commercial numerical simulators have been constructed based on solutions to these equations. These simulators have been used extensively in industrial applications such as in modelling aquifer flows, groundwater contaminant modelling and in oil reservoir engineering. However, it has proven to be particularly difficult to numerically simulate immiscible viscous fingering directly. By this, we mean that virtually all attempts to directly solve the two-phase transport equations numerically have failed to reproduce realistic viscous fingering showing all of the detail observed in experiments (Berg and Ott 2012; de Loubens et al. 2018; Bakharev et al. 2020). One of the most active and experienced groups working in this area remarked, “In agreement with existing literature, we find that Darcy-type simulations ... cannot predict the measured waterflood data. Even qualitatively, the viscous fingering patterns are not reproduced” (de Loubens et al. 2018).

There are (at least) two broad schools of thought about why it is difficult to generate realistic immiscible viscous fingers in two-phase numerical simulations. One view is that we do not have accurate enough numerical discretisation schemes which will overcome problems of simulating the complex finger morphology which emerges, due to problems such as numerical dispersion or grid orientation. Such errors are thought to lead to suppression and dispersal of the fingers. However, advanced high order spectral methods and other adaptive gridding schemes have been applied to model viscous unstable two-phase flows and although some fingering behaviour is observed, it is not as fully developed or realistic as observed in experiments (e.g. Riaz and Tchelepi 2006a, 2006b; de Loubens et al. 2018; Kampitsis et al. 2019, 2020). The second school, to which the authors

broadly subscribe, believes the problem is more likely to be with the physics and formulation of the viscous fingering problem or the algorithmic approach to the solution of the VF problem. An approach to the solution of the immiscible VF problem was proposed by the authors recently (Sorbie et al. 2020) and is described in detail in that paper and applied in subsequent work to model viscous fingering experiments in 2D slabs referred to the above (Salmo et al. 2022; Beteta et al., 2022a). In brief, this approach starts from the “observed” *fractional flow* (denoted $f_w^*(S_w)$) as the main input to the numerical simulation. However, this only specifies a *ratio* of relative permeabilities, (k_{ro}/k_{rw}), and the correct choice of these is the one that *maximises* the total mobility, $\lambda_T(S_w)$, where, $\lambda_T(S_w) = \lambda_o(S_w) + \lambda_w(S_w)$; or at least maximises $\lambda_T(S_w)$ within the constraints of the end-point relative permeabilities. Extensive discussion of this method and its application to modelling viscous-dominated 2D viscous fingering floods is given in previous publications (Sorbie et al. 2020; Salmo et al. 2022; Beteta et al. 2022a). A paper on the application of this approach to model field-scale viscous fingering and the effect of polymer flooding has appeared recently (Beteta et al. 2023).

However, the method proposed previously (Sorbie et al. 2020) only considered *the viscous-dominated* problem (i.e. where $P_c = 0$) and, in this earlier publication (Sect. 3), some justification for taking a lower stabilisation length scale due to capillarity, L_{cap} , was presented. This was identified with the fine grid where a grid size of δx would lead to a mixing length (dispersivity, α) of $\alpha \approx (\delta x/2)$. This approximation proved to be perfectly adequate to model the viscous-dominated 2D slab floods of Skauge et al. (see refs above) over a wide range of viscosity ratios of $(\mu_o/\mu_w) \sim 400\text{--}7000$ (Salmo et al. 2022; Beteta et al. 2022a) and also the core flooding results for a $(\mu_o/\mu_w) = 100$ case (Beteta, et al. 2022b). Previously, we have found the discussion by Arya et al (1988) on mixing length with system length scale to be very useful (Salmo et al. 2022). The new work presented in this paper is on the effect of including capillary effects for systems of different wettability in viscous fingering calculation.

1.3 The Inclusion of the Effects of Wettability/Capillarity in Viscous Fingering Modelling

The system wettability and capillarity are intimately related since the wetting state of the porous medium in turn affects the capillary pressure of an invading phase displacing a resident phase. The relevant contact angle for an oil/water system is denoted θ_{ow} ; however, in a porous medium it is very common that there is a distribution of contact angles within the pore space; for a discussion of this see Dixit et al. (1999) and references therein. At the macroscopic scale, there is no direct cognizance of “wettability” in our flow equations; that is, there is no single number or function we input to a standard numerical simulator representing this property. Wettability is simply (indirectly) characterised by the precise form of continuum scale capillary pressure function, $P_c(S_w)$, which we measure and use in our flow equations. Indeed, in practice it is usually the P_c function that is used to define wettability or wetting state of the porous medium, as discussed in Dixit et al. (2000). Of course, the P_c arises as a function of the medium wettability, pore structure, network connectivity and heterogeneity (variability of pore sizes, pore geometry, presence of microporosity, etc.). Equilibrium capillary pressure is defined in oil/water systems simply as, $P_c(S_w) = P_o - P_w$, irrespective of the actual wetting state of the porous medium or the nature of the invading or defending phases. The traditional definition of capillary pressure as $P_c(S_w) = P_{NW} - P_W$,

where P_{NW} and P_w are non-wetting (NW) and wetting (W) phase pressures, respectively, has largely been abandoned since we are generally considering complex heterogeneously mixed wetting state of porous media in all except the simplest systems.

It is already well known that the effect of capillary pressure, P_c , is to stabilise viscous fingers and this has been analysed in some detail using linear stability analysis; the most insightful studies in this respect are those of Yortsos and Hickernell 1989; Daripa and Pasa 2008. This raises the question of why the effect of P_c has not been well established in macroscopic simulation previously, although many simulation studies have appeared that include P_c in the calculations (e.g. Riaz and Tchelepi 2006a, 2006b; Berg and Ott 2012; de Loubens et al. 2018). The reason was referred to above, where it was noted that no studies have been able to simulate well-developed viscous fingering in the first place (i.e. for $P_c = 0$), in order to show their subsequent damping by capillarity. Since the methods we have developed gives very well-developed viscous fingers, we are in a position to study the additional nonlinear diffusive effects of capillarity (Sorbie et al. 2020).

2 Governing Equations for Two-Phase Flow in Porous Media

2.1 Transport Equations

There are several formulations of the two-phase flow equations (Peaceman 1977; Aziz and Settari 1979; Pinder and Gray 2008; Wu 2015) which are all equivalent. One coupled form of the incompressible two-phase pressure and saturation equations, including viscous, capillary and gravity terms, is as follows:

$$\nabla \cdot \left[\lambda_T \underline{k} \cdot \nabla P_o - \lambda_w \underline{k} \cdot \nabla P_c - \lambda_T (\rho_o - \rho_w) \underline{g} \underline{k} \cdot \nabla z \right] = 0 \tag{1}$$

$$\phi \left(\frac{\partial S_o}{\partial t} \right) = \nabla \cdot \left[\lambda_o \underline{k} \cdot \nabla P_o - \rho_o \underline{g} \nabla z \right] \tag{2}$$

where, with subscripts w and o referring to the water and oil phases, S_o and S_w are the phase saturations where $(S_o + S_w = 1)$, λ_o and λ_w are the phase mobilities, $\lambda_o = (k_{ro} / \mu_o)$ and $\lambda_w = (k_{rw} / \mu_w)$, λ_T is the total mobility, $\lambda_T(S_w) = \lambda_o(S_w) + \lambda_w(S_w)$, k_{ro} and k_{rw} are the relative permeabilities (RPs), ρ_o and ρ_w are the phase densities, ϕ is the porosity, \underline{k} is the permeability of the porous medium which in general may be a Cartesian tensor (although \underline{k} is usually assumed to be diagonal) and \underline{g} is the gravitational constant. For the moment, we will ignore gravity ($\underline{g}=0$) in the following development but it is included in our discussion of the scaling groups (below) for use at a later date. With $\underline{g}=0$, then the equations for viscous/capillary flow become:

$$\nabla \cdot \left[\lambda_T \underline{k} \cdot \nabla P_o - \lambda_w \underline{k} \cdot \nabla P_c \right] = 0 \tag{3}$$

$$\phi \left(\frac{\partial S_o}{\partial t} \right) = \nabla \cdot \left[\lambda_o \underline{k} \cdot \nabla P_o \right] \tag{4}$$

A clearer view of the nonlinear diffusion effect of the two-phase front is seen when the above equations are expressed in “convection–diffusion” form as follows in 1D (Stephen et al. 2001):

$$\left(\frac{\partial S_w}{\partial t}\right) = -u(S_w)\left(\frac{\partial S_w}{\partial x}\right) + \frac{\partial}{\partial x}\left[D(S_w)\left(\frac{\partial S_w}{\partial x}\right)\right] \tag{5}$$

where the convective (Buckley–Leverett) term, $u(S_w)$, and dispersive/diffusive term, $D(S_w)$, are given by:

$$u(S_w) = \frac{q}{A\phi}\left(\frac{df_{wv}}{dS_w}\right) = v_t\left(\frac{df_{wv}}{dS_w}\right) \tag{6}$$

$$D(S_w) = -\frac{k}{\phi}\left(\frac{\lambda_o\lambda_w}{\lambda_o + \lambda_w}\right)\left(\frac{dP_c}{dS_w}\right) \tag{7}$$

where the fluid velocity is given by $v_t = q/(A\phi)$. Note that the nonlinear diffusion term, $D(S_w)$, is always ≥ 0 since the derivative of the capillary pressure is always, $(dP_c/dS_w) \leq 0$. In addition, $D(S_w) = 0$ at each end point of the saturation range, since $\lambda_w = 0$ at $S_w = S_{wi}$ and $\lambda_o = 0$ at $S_w = 1 - S_{or}$; S_{wi} is the initial water saturation where $k_{rw}(S_{wi}) = 0$, and S_{or} is the residual oil where $k_{ro}(S_w = 1 - S_{or}) = 0$. Plots of this quantity, $D(S_w)$, will be presented below for the unstable viscous fingering cases simulated in this work. Equation (5) can be cast in dimensionless form by letting $T = (v_t t)/L$ and $X = (x/L)$ to obtain:

$$\left(\frac{\partial S_w}{\partial T}\right) = -\tilde{u}(S_w)\left(\frac{\partial S_w}{\partial X}\right) + \left(\frac{D_{\max}}{v_t L}\right)\frac{\partial}{\partial X}\left(\tilde{D}(S_w)\left(\frac{\partial S_w}{\partial X}\right)\right) \tag{8}$$

where $\tilde{u}(S_w) = \left(\frac{df_{wv}}{dS_w}\right)$ and is dimensionless (but not normalised) and the quantity $\tilde{D}(S_w) = D(S_w)/D_{\max}$ is both dimensionless and normalised to 1, since D_{\max} is the maximum value of the $D(S_w)$ function. The dimensionless constant term in Eq. 8 is like an inverse Peclet number (N_{Pe}), as follows:

$$N_{Pe} = \left(\frac{v_t L}{D_{\max}}\right) \tag{9}$$

and this is one expression of the viscous/capillary ratio as a *constant* in this two-phase equation. We will return to this later in our discussion of the scaling of results and also in the analysis of the numerical results.

2.2 Numerical solution of fingering including Pc

To solve the coupled viscous/capillary transport equations for two-phase flow in porous media, we use the approach proposed in Sorbie et al. (2020). That is, we choose the fractional flow, $f_w^*(S_w)$, followed by deriving the maximum mobility relative permeabilities (RPs k_{ro} and k_{rw}). A normal numerical simulation is then carried out, usually in a correlated random permeability field, using simple numerical methods, such as single point upstreaming of the convection terms. In this work, we use the numerical simulator STARS (CMG, Calgary), but any simulator model can be used without modification. The approach has been tested with the same data on several simulators which give the same answer for

our “base case” example (oil recovery, watercut and ΔP profiles, plus finger patterns and tertiary polymer response).

However, we will take as our base case example, a model which we have already simulated assuming viscous forces only (Salmo et al. 2022; Beteta et al. 2022a), and we will use these previously derived flow functions (i.e. $f_w^*(S_w)$, k_{ro} and k_{rw}) here directly. It is already known that these functions give fully developed viscous fingering which agrees very well with the experimental results. In order to assess the effect of P_c on the fingering, the equations can then be solved by simply including the chosen capillary pressure function, $P_c(S_w)$, in the simulations.

It is already well known that the solutions to the two-phase equations including viscous and capillary terms is dependent on the balance between these two forces. For example, at very high flow rates, then the viscous forces will dominate and the transport will approach the Buckley–Leverett (BL) solution (in 1D) and sharp fronts will be observed (Buckley and Leverett 1941; Peaceman 1977; Aziz and Settari 1979; Pinder and Gray 2008; Wu 2015). Correspondingly, at sufficiently slow flow rates, then capillarity will dominate and solutions will be obtained of the limiting nonlinear diffusion equation. Since we are considering the effect of the viscous/capillary force balance on viscous fingering, we now introduce the scaling groups for two-phase flow in the following section. This has already been done in a simple way by introducing the Peclet number for two-phase flow in Eq. 9 above, but this is a *single number* and the scaling of the nonlinear two-phase equations is a little more complex, as shown in the following section.

3 Force Balances and Scaling in Two-Phase Flow

3.1 Scaling Theory Following Rapoport (1955)

To study the balance of viscous and capillary forces as it affects the modelling of immiscible viscous fingering, we apply scaling theory using the formalism introduced by Rapoport (1955). This fundamental and very powerful technique has become rather old fashioned and forgotten in modern porous media research.

The broad intent of scaling theory in engineering is usually to construct a model at the laboratory or pilot scale of a much larger system, but in such a way that in a dimensionless space these two models are actually identical. This means that all the forces are identically balanced relative to each other in each system. In the context of flow through porous media, Rapoport (1955) described one system as a “prototype reservoir”, such as a laboratory flow experiment, and the scaled system as the “model reservoir”, as shown in Fig. 1. The *prototype* reservoir quantities such as total size, injection flow rates, permeabilities, etc. (i.e. Δx , Δy , Δz , q , k_x , k_y , k_z , etc.) have corresponding values in the model reservoir (i.e. $\Delta x'$, $\Delta y'$, $\Delta z'$, q' , k'_x , k'_y , k'_z , etc.). Table 1 shows the dimensionless dependent and independent quantities for both the prototype and model reservoirs. Assuming the relative permeabilities and reservoir structure remain the same, then if all the five similarity groups in Table 1 are held constant, then the prototype and model reservoirs are exactly scaled. This is equivalent to saying that in completely dimensionless variables the two systems are *identical*. For two-phase flow in 3D, there are exactly five similarity groups (see Table 1) as follows: (i) two force balances viscous/capillary (C_{VCI}) and viscous/gravity (C_{VGI}); the capillary/gravity balance (C_{CGI}) is then fixed); (ii) two “shape groups” (C_{S1} and C_{S2}) governing reservoir shape and permeability anisotropy; and (iii) the viscosity ratio (μ_o/μ_w)

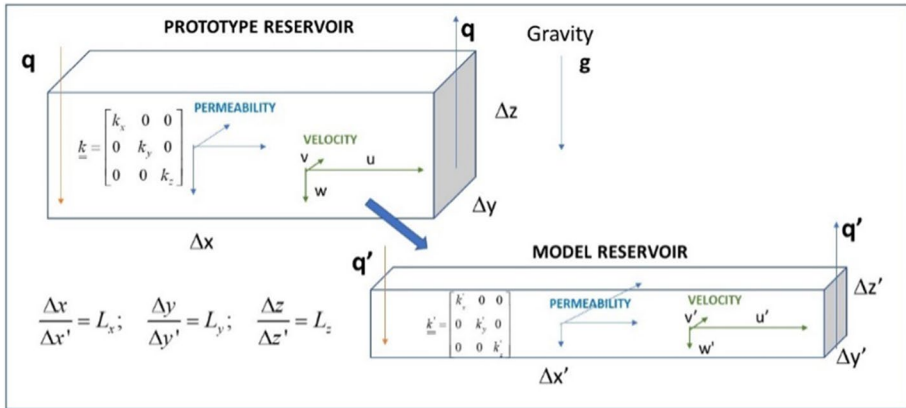


Fig. 1 Scaling between the prototype (laboratory) reservoir and the model (field) reservoir

Table 1 Scaling groups after Rapoport (1955)

Independent groups

$$\frac{x}{\Delta x}; \frac{y}{\Delta y}; \frac{z}{\Delta z}; \frac{t}{\Delta t}$$

Dependent groups

$$S_w; \frac{P}{\Delta \rho}; \frac{\text{Cum. oil recovery}}{\text{Total oil in place}}$$

Similarity groups

Force balances

$$C_{VC1} = \frac{q \cdot \Delta x \cdot \mu_o}{k_x \cdot \Delta y \cdot \Delta z \left(\frac{dP_c}{dS_w} \right)} = \frac{\text{viscous}}{\text{capillary}}; \quad C_{VG1} = \frac{q \cdot \Delta x \cdot \mu_o}{g \Delta \rho \cdot k_x \cdot \Delta y \cdot \Delta z^2 \left(\frac{dP_c}{dS_w} \right)} = \frac{\text{viscous}}{\text{gravity}}$$

Shape groups

$$C_{S1} = \frac{k_i \Delta y^2}{k_j \Delta x^2} = C_{S2} = \frac{k_i \Delta z^2}{k_i \Delta x^2}$$

And...

$$\frac{\mu_o}{\mu_w}$$

must be fixed. The reason for the subscript 1 in the force balance groups is that there are actually three forms of each of these quantities, but they are not independent and any sets can be used. Ground breaking though his paper was, Rapoport (1955) did not lay this out very clearly.

3.2 Application of Scaling Theory: The Viscous/Capillary Force Balance

For completeness, in the governing equations (Eqs. 1 and 2) we have introduced all three forces for two-phase flow (viscous, capillary and gravity). This leads to two force balances as in Table 1—but we will consider only the viscous/capillary scaling group here (C_{VC1}) since this force balance is the focus of this paper (here we assume $g=0$), and this is expressed as:

$$C_{VC1} = \frac{q \cdot \Delta x \cdot \mu_o}{k_x \cdot \Delta y \cdot \Delta z \left(\frac{dP_c}{dS_w} \right)} = \frac{\text{viscous}}{\text{capillary}} \tag{10}$$

Note that, consistent with the “convection–diffusion” formulation of the two-phase transport equation with capillarity (Eqs. 5 and 7), the C_{VCI} scaling group refers to the *slope* of $P_c(S_w)$ —i.e. to (dP_c/dS_w) —and not to the magnitude of P_c itself. This may seem like an abstruse and complicated quantity to “scale” from one system to another, but in numerical simulation calculations it is quite straightforward, e.g. If we have a function $P_{c1} = P_{c1}(S_w)$ and we double the value of the slope of P_{c1} , then we can choose $P_{c2} = 2.P_{c1}(S_w)$ which has the required property.

In fact, Eq. 10 is the more rigorous expression of the viscous/capillary force ratio as it is a nonlinear function, unlike the simpler Peclet number, $N_{Pe} = (v_i L / D_{\max})$, given in Eq. (9). N_{Pe} is a *single number* which was found by making the two-phase transport equation dimensionless. Of course, both quantities C_{VCI} and N_{Pe} will usually vary in the same *qualitative* manner, but we will show below that C_{VCI} is more useful.

Scaling theory is clearly of relevance when considering the effect of P_c on viscous fingering, since there is an obvious connection between the magnitude of the P_c effect and the viscous/capillary force balance, as represented in the group, C_{VCI} . If $C_{VCI} \rightarrow \infty$, then the system is viscous dominated (the Buckley–Leverett limit in the convection/diffusion formulation) and effectively $P_c \approx 0$. The convection/diffusion (or convection/dispersion) formulation refers to the two-phase equations of flow in porous media when cast in the fractional flow/Buckley–Leverett form including capillarity as in Eqs. (5) or (8). However, if $C_{VCI} \rightarrow 0$, then the system is capillary dominated and the system will be in a strongly (nonlinear) diffusive flow regime, and any shocks will be dispersed.

Scaling theory can also be applied in another way as we will demonstrate in more detail later in this paper; but the flavour of the application is as follows. Suppose capillarity (say a large water wet P_c) actually suppressed viscous fingering at the lab (~10–50 cm) scale for an adversity viscosity ratio flood (high μ_o/μ_w) in a porous medium. This will appear experimentally as an “almost stable” two-phase displacement, and will not show the character of well-developed viscous fingering. Indeed, such an experiment will be presented in this paper. For such a case, we may apply scaling theory by rigorously scaling up our lab system in *size* (increasing Δx in Eq. 10) but holding the (WW) P_c the *same* as the experimental curve. This means that as the size of the system increases, then C_{VCI} will increase, i.e. the viscous forces will gradually dominate and the viscous fingering will emerge at a larger scale, well above that which can be observed in the lab. That is, the viscous fingering will appear at the *field* scale but not at the laboratory scale; this is the opposite of what is sometimes said of VF (i.e. that it is “a lab-scale phenomenon”!).

We will return to the application of scaling theory later in this paper, where we will show (a) experimental results supporting what is said above, and (b) size scaling of the lab system showing emergent fingering as the system size increases.

4 Input Data for the Viscous Fingering Simulations, With and Without P_c

4.1 The Base Case Simulation

As a base case simulation example, a viscous unstable case with $(\mu_o/\mu_w)=2000$ modelled in previous work will be used here to demonstrate the effect of P_c on viscous fingering. This is taken from the direct modelling of an actual 2D slab immiscible water→oil displacement experiment showing clear fingering. This was simulated assuming only

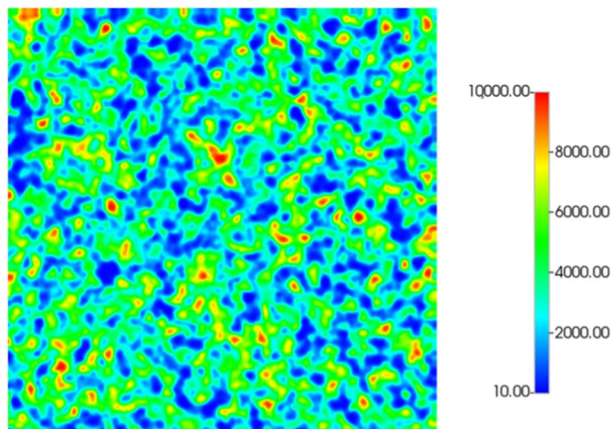
viscous forces were acting using the simulation approach described in Sorbie et al. (2020) and applied to simulate this $(\mu_o/\mu_w)=2000$ case in Salmo et al. (2022) and Beteta et al. (2022a). A brief summary of the input data set and resulting simulation match is provided here for reference, further details of the simulation are available in the original publication (Beteta et al. 2022a). Similarly, further experimental details are provided by A. Skauge et al (2012). In this paper, we prefer to refer to viscosity ratio (μ_o/μ_w) throughout rather than “mobility ratio” for reasons discussed in detail in Sorbie et al (2020) and Salmo et al (2022). However, in this earlier work, both conventional (end point) mobility ratio, M (a number), and the local mobility ratio function (especially at the Shock front, $M(S_{wf})$), are quoted (Sorbie et al 2020); Salmo et al 2022).

A resin coated 30 cm×30 cm×2.5 cm Bentheimer sandstone slab was saturated with brine, characterised for permeability and porosity before being saturated with crude oil (2000 mPa s) and aged for 3 weeks at 50 °C. By ageing the water wet Bentheimer with crude oil, the wettability was altered to oil wet or very weakly water wet (Zhou et al. 2000). The sample was then loaded into an X-ray scanner and the oil displaced with water at 20 °C at an average velocity, $v=0.44 \mu\text{m/s}$ (i.e. 0.16 cm/h or 3.8 cm/day). Following 2.5 PV of water injection, the water was viscosified to 60 mPa s with a high molecular weight co-polymer of acrylic acid and acrylamide (HPAM), and injection continued for a further 1.5 PV. The in situ finger patterns, oil recovery, water cut, and differential pressure were recorded throughout.

The subsequent simulation represented the slab with a 2D 500×500 grid with a random correlated permeability field (dimensionless correlation length, $\lambda_D=0.03$), a permeability range of 0.01–10 D and an average permeability of ~ 3 D—Fig. 2. The random correlated field has a correlation length of $\lambda_D=0.03$, representing the small scale heterogeneity present in such sandstones. The effect of larger correlation length, up to 0.4, has been presented as part of separate publications (Beteta et al. 2023; Salmo et al. 2022). When considering larger scale heterogeneity, such as layered systems resulting from fluvial deposition, another mechanism will be introduced—viscous crossflow in its traditional sense, the flow from high permeability to low permeability layers (and vice versa). Some of these large-scale heterogeneities are explored in an upcoming publication (Beteta et al. 2023).

In this paper, the main focus is to include the effects of capillary pressure (P_c) on the emergence and damping of viscous fingering across a range of length scales from the lab

Fig. 2 Simulation grid of 500×500 cells and the applied permeability field



scale to the field scale. The base case model, as noted earlier in this paper, is the viscous-dominated ($G_{VCI} \rightarrow \infty$) $m_o/m_w=2000$ case for all the experimental scale simulations; full details are given in previous papers (Salmo et al. 2022; Beteta et al. 2022a). The experiments modelled were viscous dominated and hence the experimental scale simulations had $Pc=0$. When we make $Pc \neq 0$ in our multi-scale simulations, then strictly at the lab scale there *may* be a capillary end effect, which will of course reduce as the size of the system increases. However, we view this as an *artefact* and we remove it in these simulations (at all scales). This is done simply by changing the boundary conditions or by taking a system with additional grid blocks and defining the target system as being somewhat shorter (both methods give virtually identical results). In both cases, then the outlet boundary condition is simply a constant pressure outlet and the production of each phase from the last block is the sum of the local fraction flows multiplied by the total flow rate.

Although we are mainly interested in the waterflood in this work, both the waterflood and the tertiary polymer flood were simulated, and so, recoveries, watercuts and pressure drop profiles for the whole flooding sequence are reported here.

Relative permeabilities (RPs) were generated utilising the LET correlations (Lomeland et al. 2005) to give greater flexibility in the form of the curves. As discussed above, the relative permeabilities were derived from a fixed fractional flow curve using $S_{wf}=0.19$ and maximising total mobility. The generated relative permeabilities, fractional flow and total mobility are given in Fig. 3. The relative permeabilities in Fig. 3 do not look very “conventional”, and this matter is discussed in some detail in Appendix of Salmo et al. (2022), which refers back to the earlier work of Maini and co-workers on this issue (Maini et al. 1990; Maini 1998).

The resulting simulation match to the experimental data is presented below in terms of oil recovery factor, water cut and pressure drop profiles (vs. PV) in Fig. 4, and the experimental and simulated finger patterns are shown in Fig. 5. It can be seen that an excellent match to all experimental data is obtained using this methodology. As such, this data set—with fully developed, experimentally matched, fingers—provides a sound base case from which the role of wettability/capillarity can be explored through numerical modelling.

For the viscous-dominated base case simulation, the treatment of the boundary condition (at the lab or field scale) is straightforward. The inlet flux is a fixed flow rate, and the outlet flux is the (volume conserved) oil/water flows calculated with zero capillary end effect (a total flux preserving Dirichlet condition). At the lab scale, the presence of a nonzero capillary pressure means that there may be a capillary end effect in an actual

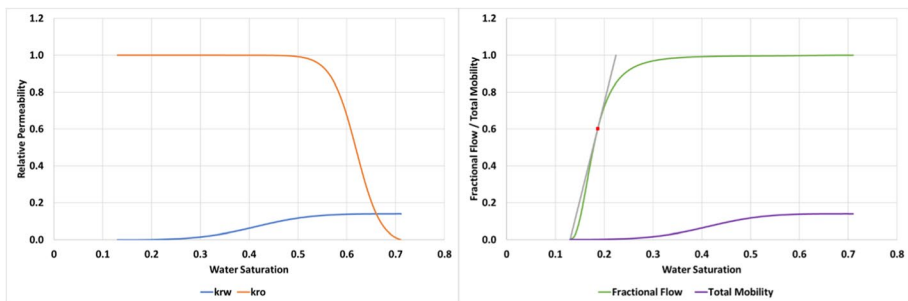


Fig. 3 Simulated 2000 mPa s slab flood—relative permeabilities (left) and fractional flow and total mobility (right)

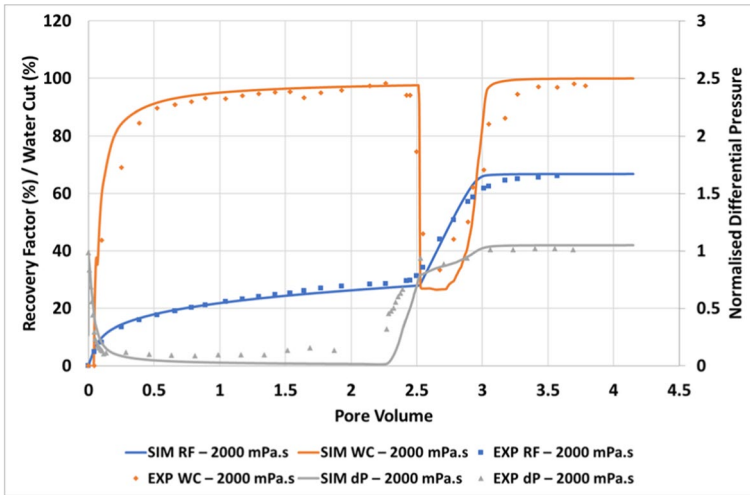


Fig. 4 Simulated 2000 mPa s slab flood (solid lines) versus experimental data (solid points)—recovery factor, water cut and normalised pressure drop

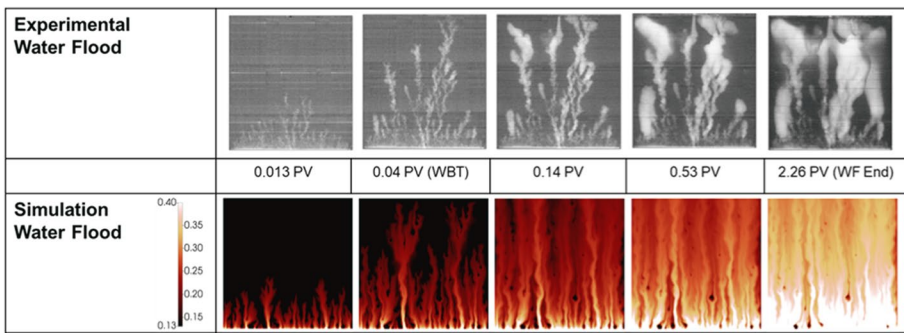


Fig. 5 Simulated 2000 mPa s slab flood (bottom) versus experimentally observed finger patterns (top)

lab-scale experiment. This experimental artefact is ignored in these simulations to bring out the main physics in the body of the system—either lab or field. Using the above boundary conditions is essentially “benign” in terms of the capillary end effect.

Given that we do not include the capillary end effect artefact (at any scale), the simulation model setup is completely routine.

The glass bead pack experiments presented in this paper are for $(\mu_o/\mu_w)=100$ in the experiments, rather than the 2000 value in the numerical example. However, in our previous papers (Salmo et al 2022; Beteta et al. 2022a, b) we have presented experiments and simulations over the entire range from $(\mu_o/\mu_w)=100$ (Beteta et al. 2022b) and then over the range from $(\mu_o/\mu_w)=400$ to 7000 (Salmo et al 2022; Beteta et al. 2022a). In terms of the instability, we see very clear immiscible viscous fingering in ALL cases including the $(\mu_o/\mu_w)=100$ case. Theoretically, as long as we can reach the viscous-dominated limit (in terms of the viscous/capillary group, $C_{VC1} \rightarrow \infty$ (large)), we will certainly see immiscible fingering. Capillarity

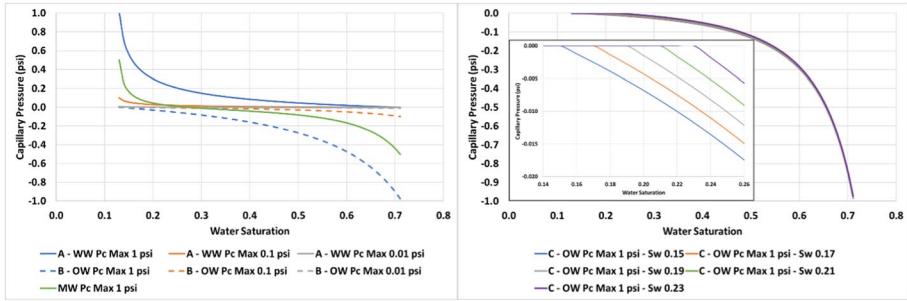


Fig. 6 Capillary pressure curves of form A, B (left) and C (right)

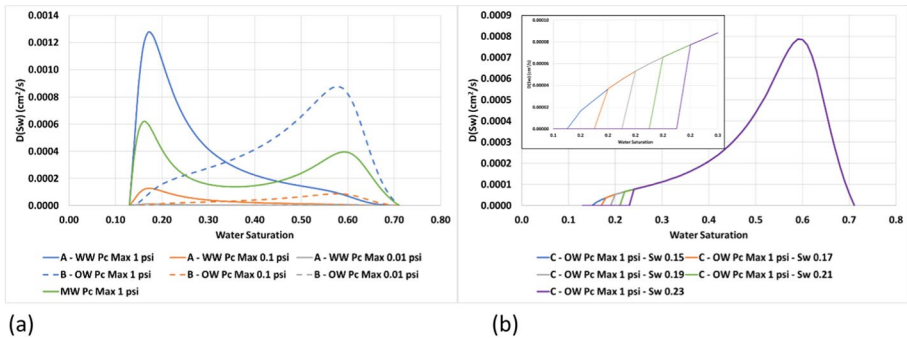


Fig. 7 $D(S_w)$ functions for each capillary pressure set—**a** Curves A and B and **b** Curve C

will have the same overall qualitative damping effect at an appropriately low value of G_{VCI} whatever the (μ_o/μ_w) ratio, although the fine details will differ a little.

4.2 Capillary Pressure Functions for Various Wetting Scenarios

As discussed above, “wettability” here is characterised by the form and characteristics of the capillary pressure function, $P_c(S_w)$. We use the abbreviations WW, MW and OW to describe water wet, mixed wet and oil wet cases, respectively. For the purposes of this work, these are defined as shown in Fig. 6. The WW P_c function shows only positive ($P_c(S_w) \geq 0$) decreasing values starting from a maximum value of $P_{c,max}$ at $S_w = S_{wi}$. All WW curves have exactly the same form and only $P_{c,max}$ is changed in the calculations; this is denoted “WW P_c ” in our calculations; Curve A in Fig. 6. The OW P_c curves all start at $P_c = 0$ at $S_w = S_{wi}$ and either (a) continuously decrease monotonically where $P_c(S_w) < 0$ to a value of $-P_{c,max}$ at $S_w = (1 - S_{or})$; this case is denoted as “continuous OW P_c ”—Curve B in Fig. 6; or (b) maintain the value of $P_c(S_w) = 0$ (or any constant value) from $S_w = S_{wi}$ to S_{wx} , followed by a continuous decrease where $P_c(S_w) < 0$ for $S_w > S_{wx}$ to a value of $-P_{c,max}$ at $S_w = (1 - S_{or})$; this case is denoted “piecewise OW P_c ”—Curve C in Fig. 6. The reason for taking these two forms of the OW P_c cases will become evident when the results are presented below. The MW case has both a positive and a negative branch as shown in Fig. 6; however, we do not show any results for this case, although we have carried out the simulations for reasons explained later.

These P_c functions lead to the corresponding $D(S_w)$ functions in Eq. 7 which appear in the flow equations; the form of $D(S_w)$ is not obvious since it also involves phase mobilities. The $D(S_w)$ functions corresponding to the various P_c curves are plotted in Fig. 7. For these specific capillary pressure functions with the highest capillary pressures ($P_{c,\max} \sim 1$ psi, in this case), the resulting $D(S_w)$ functions for both the WW and OW P_c cases have an approximate maximum value of, $D_{\max} \approx 1.3 \times 10^{-3}$ cm²/s. Recall from the above that the velocity of the base case 2D slab flood is, $v_l = 4.4 \times 10^{-5}$ cm²/s, and the system size is, $L = 30$ cm; this gives a Peclet number (Eq. 7b) of $N_{Pe} = (v_l L)/D_{\max} \approx 1$, and for such a low Peclet number (for $P_{c,\max} \sim 1$ psi), we may expect a significant effect of capillarity in this base case flood including capillary pressure of this value. The corresponding Peclet numbers for the $P_{c,\max} \sim 0.1$ and 0.01psi values are $N_{Pe} \approx 10$ and 100, respectively.

However, we also note here that this D_{\max} value occurs close to the $S_w = S_{wf}$ shock front saturation for the WW P_c case (see Fig. 7a—Curve A), but the D_{\max} for the OW P_c is at much higher S_w value, where $S_w \gg S_{wf}$ (see Fig. 7a—Curve B and Fig. 7b—Curve C). We will return to these observations later.

Considering the sensitivity of viscous fingering to wettability, then for “conventional” relative permeabilities (RPs), these functions are thought to have particular forms for water wet and oil wet systems. The new approach to immiscible fingering outlined in Sorbie et al. (2020) for the displacement of viscous oils essentially abandons the conventional idea of RPs. It takes as the primary input the fractional flow (denoted fw^*) and then calculates the corresponding maximum mobility “relative permeabilities” (RPs) which are essentially relegated to “flow functions”. This conceptual approach is fully discussed in Sorbie et al. (2020) and a full critique of the RP issue for viscous oil is given in Appendix of Salmo et al (2022), *Appendix A: Some Comments on “Experimentally Measured” Relative Permeabilities (RPs) for Unstable Immiscible Displacements*. The “RP flow functions” which the current method derives are precisely “experimental flow curves” since they give an excellent match to *all* aspects of core flood results (Beteta et al. 2022b) and also the viscous unstable slab flow results (Beteta et al. 2022a; Salmo et al. 2022).

It is known that strictly the Sor (and Swi) may depend on the force balance in the system of viscous/capillary forces; the various definitions of “Sor” are discussed in various papers (e.g. see Ryazanov et al., 2009). However, here we take the two-phase flow “standard model” of assuming that the end-point rel perms of each phase are zero; i.e. at Swi, then $kr_w = 0$ and at Sor, then $kro = 0$. Thus, irrespective of the form of the Pc curve, the phase mobilities (λ_o and λ_w) are of course also zero at these end points and therefore the $D(S_w) = 0$, as shown in the paper. In fact, the only end point that is important in this work is at the Sor end, and since no blocks actually fully reach this value due to the adverse viscosity ratio, then this point is unimportant here.

4.3 System Heterogeneity, Variable P_c and the Leverett J-function

In this work, although the permeability field is represented as a random correlated field which is of course heterogeneous, most simulation cases including WW or OW P_c functions use a single P_c curve as shown in Fig. 6. We have also performed simulations including the effect of permeability heterogeneity on capillarity by using the Leverett $J(S_w)$ -function to rescale both the WW and OW curves, which is given by Eq. 11 (Leverett 1941):

$$J(S_w) = \frac{P_c(S_w) \sqrt{(k/\phi)}}{\sigma_{ow} \cdot \cos \theta_{ow}} \quad (11)$$

where k is the local permeability, ϕ is the porosity, σ_{ow} is the o/w (oil/water) IFT and θ_{ow} is the o/w contact angle. These calculations will be presented as part of a later paper; however, we can comment here that these results including the J -function scaling of the P_c do not significantly change the conclusions of this work.

5 Viscous Fingering Simulations of Water-Wet (WW) Cases at Different Scales

5.1 Viscous Fingering at the Lab Scale: The WW P_c Case (Curve A Type)

The viscous-dominated case ($P_c = 0$), for the water \rightarrow oil displacement case for viscosity ratio (μ_o/μ_w)=2000 is presented in Sect. 4.1, and this is the base case on which the further cases including capillary pressure are based. We start by simulating the water wet (WW) P_c case (Curve A; Fig. 6) comparing this base case ($P_c = 0$) with the cases for successively higher P_c values, $P_{c,max}(S_{wi})=0.01, 0.1$ and 1 psi. The results for these four calculations are presented in Fig. 8 which shows a snapshot of the water saturation distributions at 0.04PV of injection which is the WBT (water breakthrough time) for the viscous-dominated case.

The results in Fig. 8 show that P_c values of $P_{c,max}=0.1$ or 1 psi almost completely “wash out” the fingering in these WW cases. Only when a very low $P_{c,max}=0.01$ psi is used do the fingers still clearly appear, and even this case the fingers are still visibly more dispersed than the purely viscous-dominated ($P_c = 0$) case. Clearly, a very small value of P_c , as

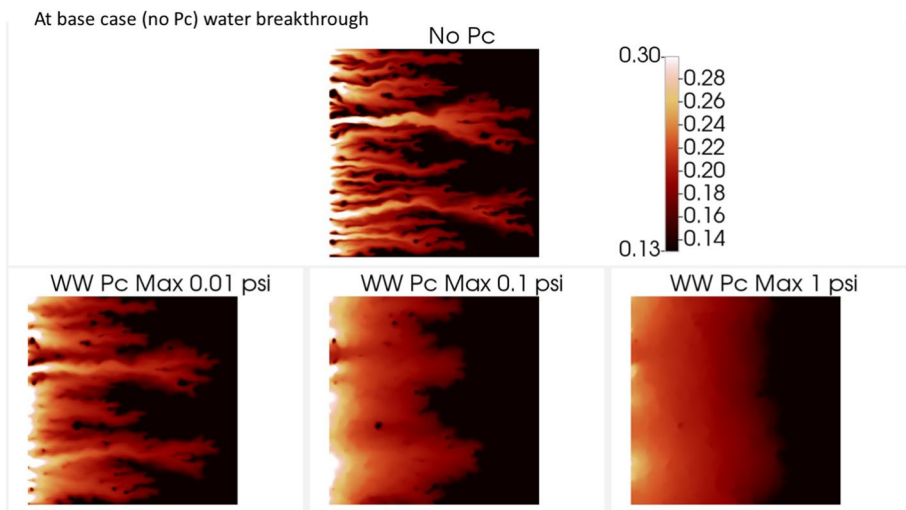


Fig. 8 Water saturation finger patterns after 0.04 PV of water injection (WBT for viscous-dominated case ($P_c = 0$)) for water wet P_c curves (type A); the corresponding Peclet numbers for the simulations including P_c are $N_{Pc} = 100, 10$ and 1 for the cases with $P_{c,max}(S_{wi})=0.01, 0.1$ and 1 psi, respectively

manifested through the $D(S_w)$ function, can disrupt the formation of viscous fingers by damping them out. This finger spreading occurs both in the direction of flow in these linear 2D floods and in the transverse direction. Recall from the above that the values of the calculated Peclet number for the three cases in Fig. 8 were $N_{Pe} \approx 1, 10$ and 100 , for the cases with $P_{c,max} = 1, 0.1$ and 0.01 psi, respectively. Based on these values of N_{Pe} , we might qualitatively expect the lowest capillary pressure case to show some degree of fingering. We noted above that the value of the shock front saturation in the viscous-dominated flood ($P_c = 0$) is $S_{wf} = 0.19$, and it is probably the magnitude of the $D(S_w)$ function at this saturation value that is important, and this will be confirmed below.

The corresponding calculated profiles of cumulative oil recovery, watercut and pressure drop vs. PV—in addition to the response of the application of polymer viscosified water at 2.3 PV (polymer viscosity $\mu_p = 60$ mPa s)—are shown in Fig. 9. It is interesting that, despite the differences in fingering patterns, this shows that all four cases give similar results for all calculated quantities for both the waterflood and the polymer flood, with the purely viscous case ($P_c = 0$) having a slightly lower cumulative oil recovery. However, this is partly a result of the choice of scale here. The inset plot shows the water cut at early time (breakthrough). These clearly show some differences, and the actual breakthrough time is an important feature of any calculation. Thus, it would not be correct to say the fingering does not affect recovery. This may be a little surprising but, in applying our VF ($f_w^* / \max. \lambda_T(S_w)$) methodology, we have found that the key factor governing the final results is the choice of f_w^* and the corresponding max mobility relative permeabilities (RPs). In modelling the viscous-dominated experimental floods (Beteta et al. 2002a), we have also found that these factors (f_w^* and $\max. \lambda_T(S_w)$) can also accurately predict the response to the tertiary polymer. We also note from Fig. 9

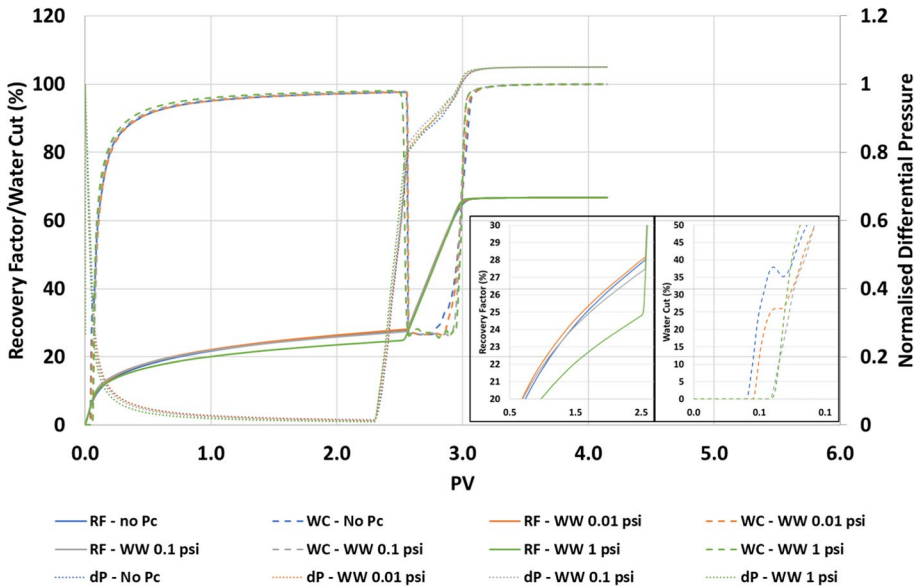


Fig. 9 Oil recovery factor, water cut and normalised differential pressure for the no Pc case as well as the three water wet (Pc curve A) cases. Inset plot showing changes in water flood recovery (left) and water breakthrough (right)

that the response of the system to the application of tertiary polymer is also almost identical for all cases, in terms of oil recovery and watercut profiles (vs. PV injected). The first conclusion from these calculations is that for a WW system, then water \rightarrow oil displacements even with a very high (μ_o/μ_w) ratio (2000 in this case), then very low levels of capillary pressure can wash out viscous fingering at the lab scale, and this appears to be correct. In the following section, we present experimental results which support this finding. A further conclusion from this WW P_c calculation might appear to be that we would then not expect to see any viscous fingering at the larger (field) scale, but this is incorrect as we will demonstrate in Sect. 5.3.

5.2 Experimental Verification of VF Suppression in WW Bead Packs

An immiscible water \rightarrow oil displacement experiment with (μ_o/μ_w) = 100 was carried out in this work as part of our immiscible viscous fingering (VF) experimental programme. The pack is a Perspex (Plexiglass) walled container with a porous medium pack size 8cm x 49cm and 0.5cm (width–length–depth) which is packed with ballotini beads with a diameter size distribution \sim 150–250 μm . As supplied and washed, the beads are quite strongly water wet and this was tested qualitatively by noting that a drop of water placed on the pack was immediately imbibed. The pack at 100% water saturation (distilled water) was flooded with $\mu_o = 100$ mPa s (clear) mineral oil which displaced the water in a very stable manner leaving an initial low water content of \sim 2–3% (by volume balance). The initial condition of the pack before waterflooding was then $S_{oi} \sim 0.97$ –0.98 of clear 100 mPa s mineral oil and $S_{wi} \sim 0.02$ –to 0.03. At this point, blue dyed water of viscosity $\mu_w = 1$ mPa s was injected to displace the $\mu_o = 100$ mPa s clear oil. The displacement sequence is shown in Fig. 10 where two groups of $12 \times$ time snapshots are shown in this figure as follows: (i) in Fig. 10a on the left, the early time displacement profiles to 0.24PV are shown in 0.02PV time steps from top left to bottom right (i.e. up to $12 \times 0.02 = 0.24$ PV of injection); (ii) in Fig. 10b on the right, the later time displacement profiles to 0.96 PV are shown in 0.08PV time steps from top left to bottom right (i.e. up to $12 \times 0.08 = 0.96$ PV of injection). The video of this flood is given in the ancillary uploaded material supplied with the paper (supplementary 1).

The most important observation here is that although we might expect to see immiscible viscous fingering for this (μ_o/μ_w) = 100 viscosity ratio, the front is only slightly distorted with no obvious evidence of instability; see Fig. 10. Indeed, this displacement could be due to a slight amount of permeability heterogeneity in the pack. A second important observation (from Fig. 10b) is that the water breakthrough (WBT) is between frames 5 and 6 in this figure—i.e. between 0.4 and 0.48PV of water injection, i.e. WBT at \sim 0.44PV; that is, at WBT the average oil saturation in the pack is $S_o \sim 0.5$ (since S_{wi} was so low). This implies that the S_w front height at the shock is around $S_{wf} \sim 0.32$ –0.4, typical of what a 1D displacement might calculate for this viscosity ratio.

We conjecture here (and later prove) that this behaviour is due to capillary pressure in this water wet (WW) system. The WW P_c stabilises the front sufficiently such that the water finger width is of order or somewhat larger than the pack width (8cm). Using the Young–Laplace equation, $P_c(S_w) = (2\sigma_{ow} \cdot \cos \theta_{ow}/r)$, and assuming $\sigma_{ow} = 25$ mN.m and $\cos \theta_{ow} \sim 1$, and estimating the average pore size, $\langle r \rangle$, in our pack of beads with diameter range 150–250 μm to be in the range $\langle r \rangle \sim 40$ to 60 μm , this would give a P_c value of $P_c \sim 1250$ –850 Pa (i.e. $P_c \sim 0.18$ –0.1 psi). Given that the permeability of this pack is $k \sim 35$ D, then this magnitude of P_c is more than enough to damp out fingering.

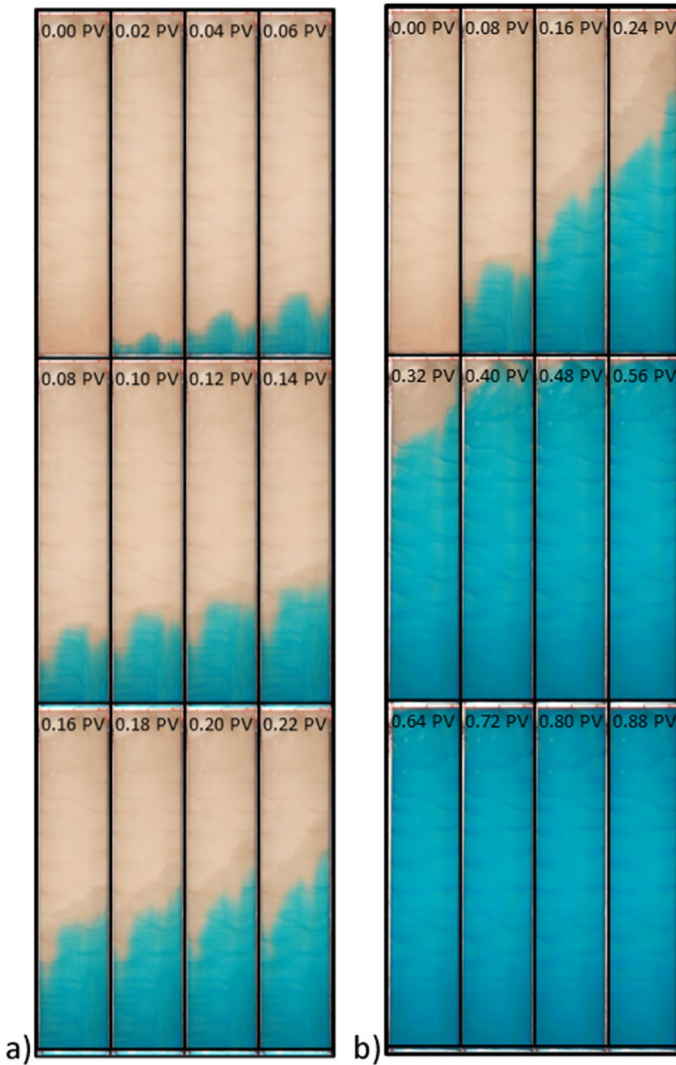


Fig. 10 Displacement of 100 mPa s (clear) oil by (blue dyed) 1 mPa s water in a water wet bead pack; **a** early time in 0.02 PV increments (up to 0.22PV) and **b** later time in 0.08 PV increments (up to 0.88PV),

We now show that, although one might think that this implies that, if no immiscible fingers are observed in a lab experiment, then none will be seen at the field scale, is incorrect. Whether or not viscous fingers will appear is a matter of length scale of the system, as will be shown using scaling theory in the next section.

5.3 Viscous fingering simulations at the field-scale WW P_c case: applying scaling theory

In the light of the simulations of immiscible fingering, and its damping by capillary forces in WW systems, we now apply scaling theory to examine the size scaling of these

initial findings, again basing our calculations on the $(\mu_o/\mu_w)=2000$ base case above. The capillary pressure, $P_c(S_w)$, is a local function, and as we go from the lab scale to the field scale, it does not change, under the usual assumptions of the flow equations in porous media. That is, the related function $(dP_c(S_w)/dS_w)$ also remains constant with length scale. Therefore, consider the form of the viscous/capillary scaling group, C_{VC1} , (Eq. 8) as follows:

$$C_{VC1} = \frac{q \cdot \Delta x \cdot \mu_o}{k_x \cdot \Delta y \cdot \Delta z \left(\frac{dP_c}{dS_w} \right)} = \frac{V \cdot \Delta x \cdot \mu_o}{k_x \left(\frac{dP_c}{dS_w} \right)} \quad (12)$$

where we identify the fluid velocity, $V = q/(\Delta y \cdot \Delta z)$ as the average fluid velocity (this flow field by definition is kept the same throughout the model with size scaling, even for a 3D system). Thus, suppose we evaluate this group for a WW P_c case at the lab scale where the viscous fingering is highly suppressed, e.g. as in the WW P_c case above with $P_{c,max} = 1$ psi (see Fig. 8). For this laboratory system, the viscous/capillary scaling group is a number, say ζ , Eq. 13.

$$C_{VC1_LAB} = \zeta = \left(\frac{V \cdot \Delta x \mu_o}{k_x (dP_c/dS_w)} \right)_{LAB} \quad (13)$$

We can see that if we simply make the system larger, i.e. increase Δx , then viscous/capillary force balance increases linearly with Δx . Note that to keep the system otherwise scaled, there is also a “shape group” (see Table 1) that must also be honoured (Eq. 14), as follows:

$$C_{S1} = \frac{k_x \Delta y^2}{k_y \Delta x^2} \quad (14)$$

However, this shape group criterion is easily dealt with if all k_x and k_y in every grid block and the exact shape of the system is maintained. As the system is expanded in size by a factor of say α , that is, the system lab system size Δx is expanded to $\alpha \cdot \Delta x$, the new value of C_{VC1} is clearly given by Eq. 15:

$$C_{VC1} = \alpha \cdot \zeta \quad (15)$$

and the viscous/capillary ratio increases accordingly. Thus, we can examine effect of simply “inflating” the system which increases the viscous/capillary scaling group in a completely consistent manner. This is shown for the laboratory-scale example in Fig. 8, where we show the simulation as the size is increased by a series of “inflation” factors α_1, α_2 , etc., as shown in Fig. 11.

From the results in Fig. 11, it is clear that, although the immiscible fingering in a WW system may be suppressed by capillary forces at the laboratory scale, it simply “emerges” at the larger scale. In the example presented in Fig. 11, the fingers emerge quite clearly at the scale of about $\Delta x \approx 30$ m ($C_{VC1} = 100\zeta$). As the system is inflated to the field scale ($\Delta x = 300$ m; where $C_{VC1} = 1000\zeta$), the fingering is almost indistinguishable from the viscous-dominated cases. Note that the lab- and field-scale cases—as shown from scaling theory—are actually absolutely identical in the purely viscous force case ($P_c = 0$) as shown in Fig. 11 (two top right cases). This assumes that the permeability structure and gridding

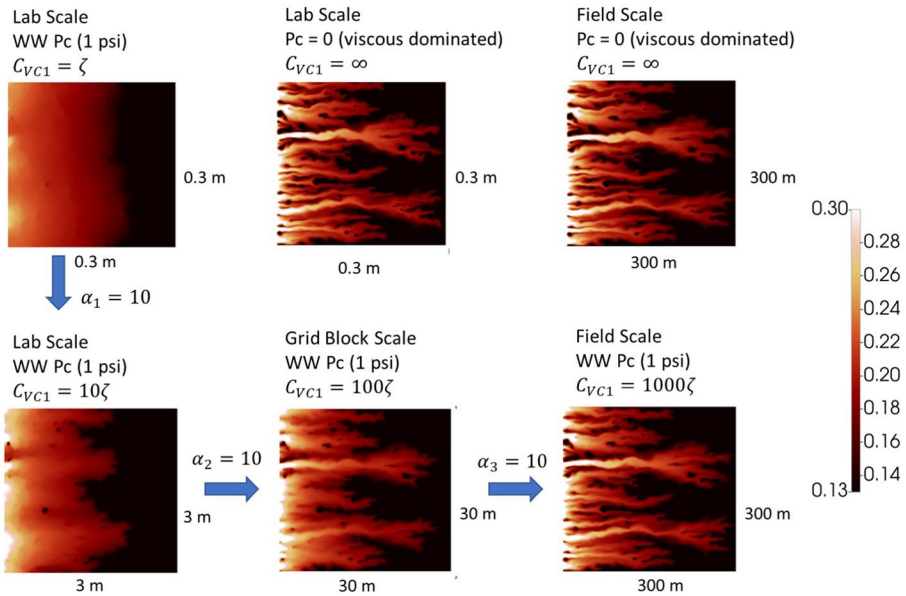


Fig. 11 Water saturation finger patterns with and without WW Pc across a range of system size inflation factors ($\alpha_1, \alpha_2, \alpha_3$, etc.)

are identical; i.e. that the *dimensionless* fluid mixing lengths are the same. This is evident from scaling theory which shows that only the shape group (C_{S1}) needs to be preserved.

We note that if we had kept WW Pc lab-scale case at exactly the *same size* (top left Fig. 11; 0.3 m x 0.3 m), then the *identical* figures for the 10zeta, 100zeta and 1000zeta scaling in Fig. 11 are produced by simple increasing V by exactly the same α_1, α_2 and α_3 factors. This is evident from the C_{VC1} group in Eq. 13 which shows that the sensitivity to Δx and V are identical; we have carried out these calculations, but the results are not presented here since they are *identical*.

Before proceeding, we also comment on the issue of fingering at the *experimental* and *field* scales. It is evident from the above simulations (and those to come), the two possible lab-scale observations are that we either *do* or *do not* observe viscous fingering. If fingering is observed then it *will* also occur at the larger scale assuming that the system dispersivity scales with lengthscale no worse than say as referred to by Arya et al (1988). It is hard to conceive of (geological) cases where this would not be qualitatively true, and viscous fingering would be observed at some higher lengthscale. If viscous fingering is *not* observed at the lab scale, then this may mean that the capillary forces are simply too big, and if this is the cause, fingering would again emerge a larger scales. If the reason for the lack of lab-scale fingers is that the system is simple already stable, then probably no fingering would emerge at the larger scale, although “channelling” may occur which bears some resemblance; but in general the matter is open*. There are further issues with boundary conditions which is a topic too general for discussion here, but suffice it to say that, in this work, the boundary conditions are taken as being “very similar”, which may or may not be the case as a real system goes from the lab to field scale. *Although he matter is “open” in for the general case, this

paper proposes most of the concepts and numerical tools required to decide what the case actually is for any given set of mathematical assumptions e.g. exact nature of the mixing with lengthscale, the boundary conditions, the pattern of heterogeneity, etc.

6 Viscous Fingering Simulations for Oil Wet (OW) P_c Cases

6.1 VF Simulations for Continuous OW P_c Curves (Curve B Type)

We now consider the modelling of oil wet (OW) systems using the same base case laboratory-scale model as used for the WW case (see Sect. 5). The simulations presented in this section use the continuous OW P_c curves shown as curve B in Fig. 6. This starts at $P_c(S_{wi})=0$ and slowly curves to a negative P_c at a lowest value at $S_w = (1 - S_{or})$ as specified; this is referred to as the maximum value, $P_{c,max}$, although strictly it is actually $|P_{c,max}|$, as explained in Sect. 4.2. N.B. $P_c(S_{wi})$ could start at any value $P_c(S_{wi}) = C$ (where C may be positive or negative) and decrease as in the continuous Curve B case.

Figure 12 shows a snapshot of the saturation distributions at 0.04PV of injection (WBT) for the viscous-dominated ($P_c = 0$) case and for the OW cases with $P_{c,max}=0.01, 0.1$ and 1 psi (negative values). It is immediately clear from these results that the OW P_c does cause some stabilisation of the fingers, just as in the WW case. So, capillarity is a finger suppressing mechanism for any wettability state. However, observing the OW simulations in Fig. 12, we note that the degree of capillary suppression of the fingers is much less for the OW case than for the corresponding WW case. Even the (negative) $P_{c,max} = 1$ psi case still shows some remnant fingers which are identifiable (unlike the WW fingers which are completely washed out). Referring to the $D(S_w)$ functions for the OW P_c cases in Fig. 12, we can calculate the Peclet numbers for the three cases as $N_{Pe} \approx 150, 15$ and 1.5 for the $P_{c,max}=0.01, 0.1$ and 1 psi, respectively. These are slightly higher than the N_{Pe} values for

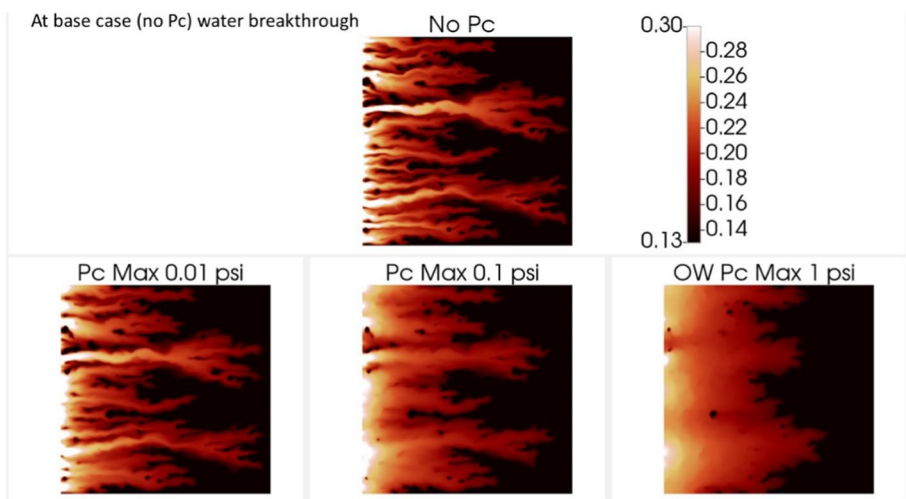


Fig. 12 Water saturation finger patterns after 0.04 PV water injection (WBT for the viscous-dominated case) for the oil wet (OW) P_c curves (type B)

the WW P_c cases, but the changes in finger patterns are much more significant than these small increases should indicate.

It soon became evident that the reason for this difference between the WW and OW cases is that the corresponding capillary diffusion term, $D(S_w)$, was lower in the region of low water saturation, since the OW P_c curve (Curve B) was closer to zero and almost flat in the region, and hence (dP_c/dS_w) is small (see Fig. 7). Specifically, we conjectured that the important issue in determining the finger suppression by capillarity is the value of this quantity ($D(S_w)$) in the region of the viscous-dominated ($P_c = 0$) shock front saturation, $S_w = S_{wf}$. We will confirm this is the case in the next subsection.

For the viscous-dominated and the OW cases in Fig. 12, Fig. 13 shows the corresponding oil recovery, watercut and pressure profiles vs. PV. Again, as for the WW cases, these OW cases agree remarkably closely in all these other aspects, i.e. the overall averaged recoveries, etc., are all very similar. Also, the incremental recovery by the application of tertiary polymer is almost identical in each case.

It is clear that carrying out the same rescaling exercise as presented for the WW case in Sect. 5.3 for the OW case will give qualitatively very similar results. That is, as the OW P_c is held constant and the system is “inflated” (as in Fig. 11), then viscous fingers would again emerge at the larger length scale. In fact, if we compared this OW P_c case in Fig. 12 with the WW P_c case above, then the OW fingers would clearly emerge “earlier”—that is at a smaller system size—than the WW fingers. We do not show these results here, since we take this as being obvious to the reader.

Before presenting a more detailed analysis and implications of these findings, we will present the results for OW systems of the type shown in Curve C (Fig. 6) and the experimental results for the OW system.

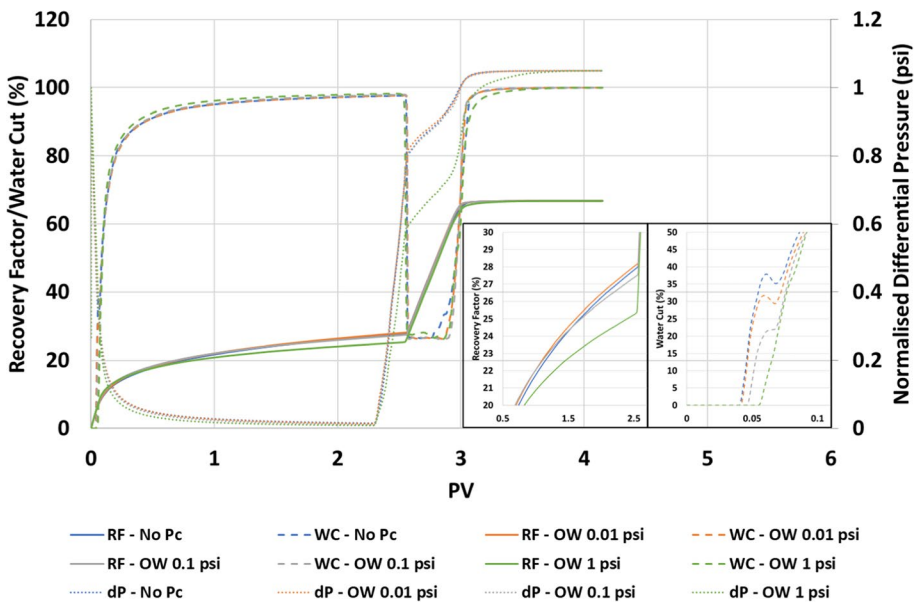


Fig. 13 Oil recovery factor, water cut and normalised differential pressure for the no P_c and the three oil wet (Curve B) cases. Inset plot showing changes in water flood recovery (left) and water breakthrough (right)

We also note here that we have performed further simulations for the mixed wet case (MW), but this also caused the same effects as the WW and OW cases, and these MW simulations are not presented here.

6.2 VF simulations for piecewise OW P_c curves (Curve C type)

In this section, we set out to test the conjecture that, in an OW system, the exact saturation point, $S_w = S_{wx}$, at which the PC slope (dP_c/dS_w) deviates from 0 (or a very small value) relative to the Buckley–Leverett (BL) shock front height (S_{wf}) is an important factor in finger stabilisation in OW systems. Indeed, the generalisation of this is that the value of $D(S_w)$ at $S_w = S_{wf}$ is always important.

In order to achieve the above goal, the simulations presented in this section use the piecewise OW P_c curves shown as curve C in Fig. 6. In this form of the P_c curve, the P_c is identically 0 (or constant) up until the value of $S_w = S_{wx}$, beyond which it then reduces to some lower $P_{c,max}$ (i.e. $\text{Max} | P_c |$). In the base case example, we have noted that the $S_{wi}=0.13$ and that the shock front height is $S_{wf}=0.19$ (see Fig. 6), so we use Curve C OW P_c functions with chosen values of where the P_c function goes below 0 at, $S_{wx}=0.15, 0.17, 0.19, 0.21$ and 0.23 and in all cases, we take the largest negative $P_{c,max}=1$ psi. Figure 14 shows the water saturation distributions at WBT (0.04PV) for these five cases compared with the viscous-dominated ($P_c = 0$) case and the continuous OW Curve B case (again with $P_{c,max}=1$ psi). The corresponding oil recovery factors, water cuts and normalised differential pressures are shown in Fig. 15.

Before discussing these results, we note that the Peclet number, as defined in Eq. 9, is actually *the same* for all of these cases with nonzero P_c in Fig. 14. The calculated N_{Pe} from the $D(S_w)$ function in Fig. 14 (b) is $N_{Pe} \approx 1.7$ (very similar to the previous OW and WW cases with $P_{c,max}=1$ psi). Therefore, considering only this number is clearly quite inadequate to distinguish between different cases which show fingering or highly dispersed behaviour.

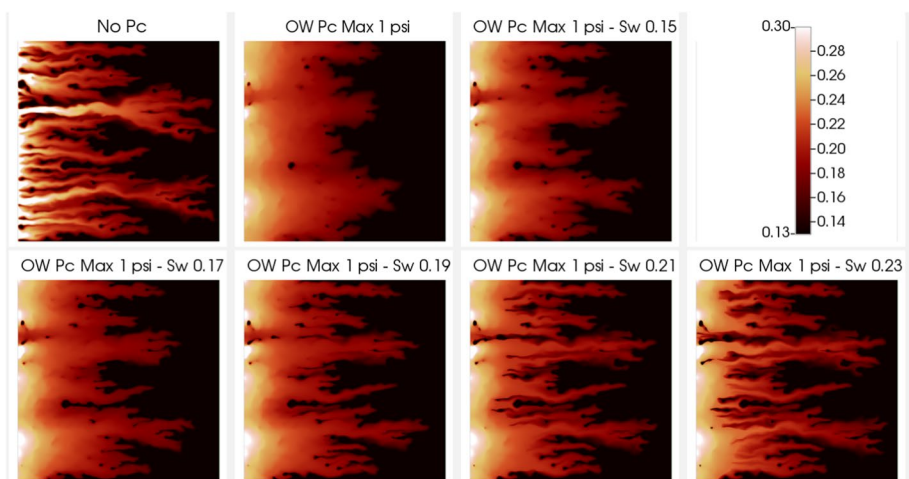


Fig. 14 Water saturation finger patterns after 0.04 PV water injection (WBT for the viscous-dominated case) for the oil wet P_c curves (type C) vs no P_c and type B (1 psi) cases

The first important result is that the two cases in Fig. 14 with $S_{wx} = 0.21$ and 0.23 (i.e. $> S_{wf}$) show quite fully developed viscous fingering, which is still visibly slightly different from the viscous-dominated ($P_c = 0$) case. In these two cases, the changes in the water saturations distributions (compared with the $P_c = 0$ case) are seen well behind the shock front, closer to the inlet side of the system. However, these two cases, if observed in an experiment would be considered to show clear well-developed viscous fingering. Turning to the cases with $S_{wx} = 0.15$ and 0.17 ($< S_{wf}$), we can see that the finger structure is in the transition towards being dispersed, with the 0.15 case being much closer to the continuous OW P_c case (curve B). These results confirm our conjecture that the position of the point S_{wx} relative to the shock front S_{wf} is of key importance in the capillary suppression of viscous fingers. We believe that this has not previously been observed.

In terms of recovery, water cut and pressure drop, it can be seen from Fig. 15 that there is a modest impact of any of the introduced capillary pressure curves—other than a slight reduction in pressure during the initial injection of viscosified brine.

All of the results in this paper so far will be analysed in more detail in discussion section. We now go on to present experimental results on the OW P_c case, which is fully consistent with the above finding.

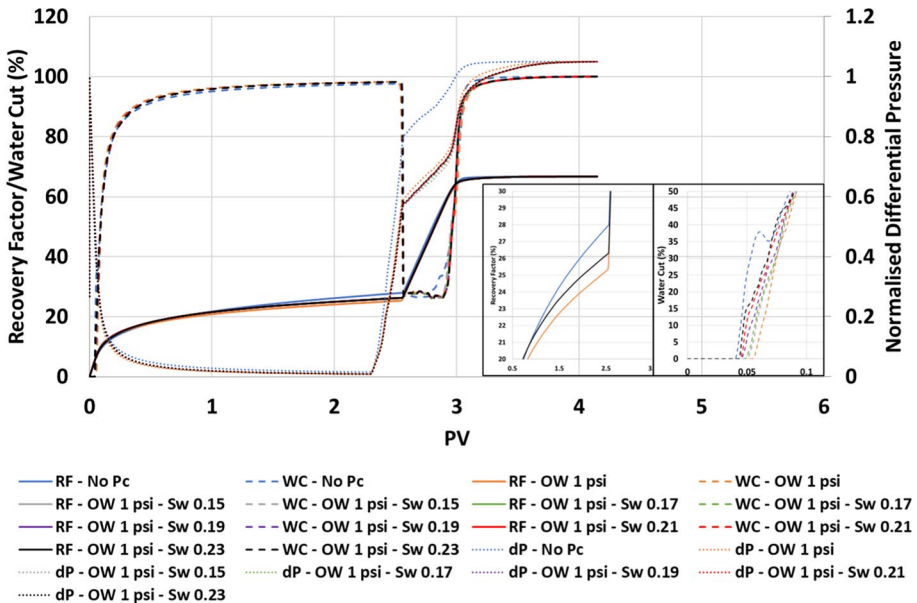


Fig. 15 Oil recovery factor, water cut, and normalised differential pressure for the oil wet P_c curves (type C) vs no P_c and type B (1 psi) cases. Inset plot showing changes in water flood recovery (left) and water breakthrough (right)

6.3 Experimental verification of oil wet (OW) viscous fingering for $(\mu_o/\mu_w)=100$

To support the assertions above about the occurrence of viscous fingering in oil wet (OW) systems, we present an OW unstable immiscible pack flood, in the same experimental setup as for the WW case in Sect. 5.2, again with viscosity ratio $(\mu_o/\mu_w)=100$. To make the porous medium oil wet, the ballotini beads were treated with trichloro (octadecyl) silane. The wettability adjustment method followed a modified version of the procedure by Hobrook and Bernard (1958), whereby the glass beads were saturated in a 5% trichloro (octadecyl) silane in decane solution for a period 24 h before being washed with 100% decane and then mineral oil.

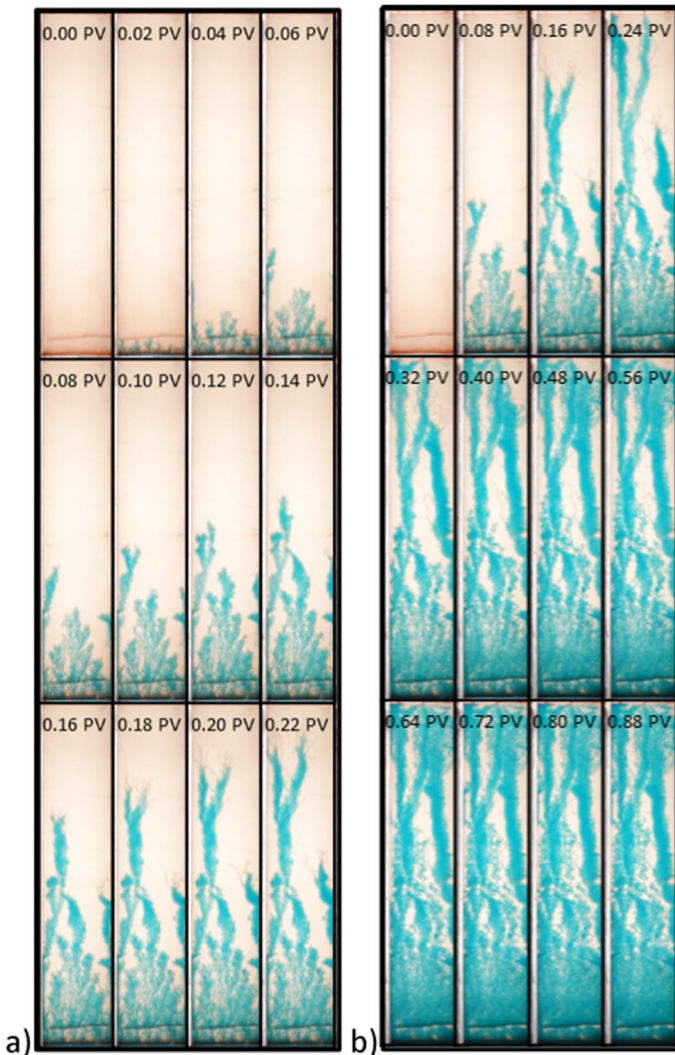


Fig. 16 Displacement of 100 mPa s oil by 1 mPa s water in an oil wet bead pack. **a** Early time in 0.02 PV increments and **b** later time in 0.08 PV increments (right)

To check the wettability, we noted that water formed a clear non-wetting drop on the oil wet beads but that mineral oil would readily spread on it and imbibe into the bead slurry. The OW pack was then reassembled in the same system as the WW case (Sect. 5.2) and flooded with clear mineral oil with viscosity, $\mu_o = 100$ mPa.s, which was carried out in the absence of water, so the pack initially has $S_{wi}=0$ and $S_{oi}=1$. Blue dyed water with $\mu_w=1$ mPa.s was then injected, giving $(\mu_o/\mu_w)=100$ at a constant velocity of 3 m/day.

Figure 16 shows the successive snapshots of the early (to 0.24 PV) and slightly later (to 0.96 PV) period of the water injection in this OW system, using the same time increments as in the earlier WW case.

The most important result in Fig. 16 is that very clear and well-developed viscous fingering is observed for this OW adverse viscosity ratio case right from the start and that water breakthrough (WBT) occurred at ~ 0.3 PV, which is significantly earlier than in the WW case, where WBT was at ~ 0.44 PV. A more subtle feature of this OW VF case is revealed by observing that at the inlet end (bottom) of the system, the (blue) water saturation is clearly spread across the near-inlet pack. This implies that there is a negative branch of the OW Pc curve for this system (which we did not measure), since the generic behaviour of this system is very similar to the OW PC case where $S_{wx} > S_{wf}$ (see Fig. 14). A video of this flood is available in supplementary 1.

7 Summary, Discussion and Conclusions

7.1 Summary of the Study

This paper presents a study of immiscible viscous fingering in a two-phase system where water displaces oil in a porous medium including the effects of wettability/capillarity. Previous work from the authors presented a novel method for modelling viscous fingers directly which correctly reproduced the complex fingering patterns seen in immiscible 2D unstable two-phase *viscous-dominated* displacement experiments in 2D rock slabs (Sorbie et al. 2020; Salmo et al. 2022; Beteta et al. 2022a). The original method solved the viscous fingering problem for the purely viscous-dominated case, where the viscous /capillary scaling group, C_{VC1} , was effectively infinite. In this paper, we take the flow function derived from our method to be the viscous-dominated quantities we require. Since it has already been shown that these flow functions will give well-developed viscous fingering, they were therefore used to study the degree of finger suppression by capillary forces as the viscous/capillary balance decreases. The three novel aspects of this work are as follows:

The effects of P_c on fully developed viscous fingering is demonstrated using direct numerical simulation for both WW and OW systems. The qualitative aspects of the WW and OW systems are shown to be different. As observed experimentally, viscous fingering is predicted to occur much more readily in an OW system—i.e. fingers are more suppressed in a WW system—and the primary reason for this behaviour is explained. The choice we make of Pc curves in this paper is quite general showing the main characteristics of WW, OW and MW systems (MW results not shown). It is the relative size of the terms $\left(\frac{1}{N_{Pe}}\right)\tilde{D}(S_w)$ vs. $\tilde{u}(S_w)$ (see Eqs. (8) and (9) for N_{Pe}) that is important. Later, we will show that the relative value of these terms close to the BL shock front ($S_w=S_{wf}$) is of particular importance.

Scaling theory, following Rapoport (1955), is applied in a novel way to show the scale dependence of immiscible fingering in porous media. Even the highly suppressed fingering of a lab-scale WW Pc system emerges quite clearly at some larger scale, as the viscous/capillary scaling group, C_{VC1} , increases from its value at the laboratory scale.

Experimental results for WW and OW water→oil displacement experiments for adverse viscosity ratio floods with $(\mu_o/\mu_w)=100$, in a ballotini pack are presented which qualitatively support our numerical findings.

7.2 Discussion of Results

For the first time, a macroscopic simulation study including clear viscous fingering in the viscous-dominated limit ($C_{VC1} \rightarrow \infty$) is presented demonstrating the effects of wettability/capillarity on WW and OW systems. It is found that viscous fingering is more suppressed in WW systems than in OW systems and this corresponds well with experimental observation both in the literature (Zhao and Mohanty 2019; Zhao 2020) and in the experimental evidence presented in this work.

Wettability and viscous fingering In explaining this difference between WW and OW systems, we first conjectured and then demonstrated that the key factor was the magnitude of the nonlinear diffusion term, $D(S_w)$, in the region of the BL shock front (where $S_w = S_{wf}$), and this is shown schematically in Fig. 17. This figure shows the BL shock front in the S_w/x profile at a given time indicating the saturation value at the shock, $S_w = S_{wf}$ (Fig. 17a). The Type C piecewise OW P_c curve is shown schematically (Fig. 17b), where the region between $S_{wi} \leq S_w \leq S_{wx}$ is very “flat”, it is shown as about zero in this figure ($P_c \approx 0$), but it simply needs to be *constant*, so that $(dP_c/dS_w) \approx 0$. Hence this leads to the form of the nonlinear diffusion term due to capillarity, $D(S_w)$, being almost zero in this region (i.e. $S_{wi} \leq S_w \leq S_{wx}$), as shown in Fig. 17c. In the region $S_{wx} \leq S_w \leq (1 - S_{or})$, the P_c curves become successively more negative and the value of $(dP_c/dS_w) \neq 0$ (negative) and initially increases (gets more negative) with S_w , and hence $D(S_w) > 0$ in this region. This quantity must show a maximum and then limit to $D(S_w)=0$ at $S_w = (1 - S_{or})$ since the oil mobility (λ_o) becomes zero at this point (Eq. 7). Finally, depending on whether the front height S_{wf} is greater or less than the value of S_{wx} , then distinctly different behaviour is observed. If $S_{wf} < S_{wx}$, then the effect of capillarity at the front is small and hence the fingers can form in a manner very similar to the viscous-dominated case. The effect of $D(S_w)$ only occurs some distance *behind* the front where it has the effect of merging the fingers in that region and giving an area of more dispersed S_w . If $S_{wf} > S_{wx}$, then the capillary effect strongly disperses the incipient viscous fingers in the region of the shock front and very effectively hinders the fingers from forming. Both of these are indicated in Fig. 17d where an example of the 2D water saturation distribution, $S_w(x, y)$, is shown; the upper $S_w(x, y)$ pattern in this figure is for the case of $S_{wf} < S_{wx}$, and the lower one is for $S_{wf} > S_{wx}$.

Scaling and viscous fingering As long as the simulation actually produces viscous fingers for the viscous-dominated ($P_c=0$) case, scaling theory using the viscous/capillary scaling group, C_{VC1} , (and the appropriate “shape group”, C_{S1}) shows that as the size of the system increases, these fingers will emerge. This always occurs, even if the fingers cannot be seen at the lab scale, which is most likely the case for a water wet (WW) system. The corollary is also true, that if we observe immiscible fingering in the lab system, then the system is most likely to be oil wet (OW) or very close to neutral wet where $(dP_c/dS_w) \approx 0$.

In summary, this rescaling methodology points very logically to at least two major conclusions: (i) since the effect of the Pc (WW, OW or MW) will *always* reduce with length scale as

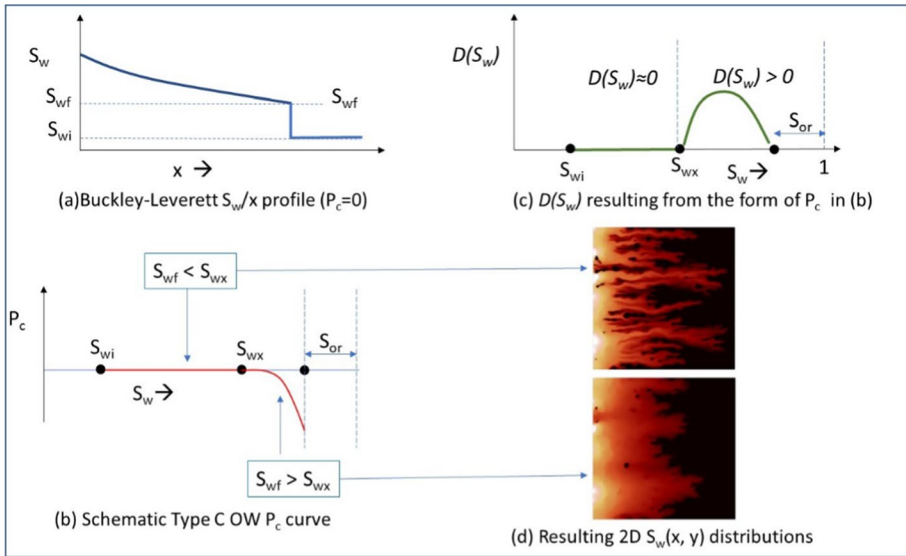


Fig. 17 Schematic representation of **a** the Buckley–Leverett saturation profile; **b** the type C P_c curve; **c** the $D(S_w)$ function; and **d** the resulting water saturation finger patterns

the system increases, then at any adverse viscosity ratio (let us arbitrarily say $(\mu_o/\mu_w) > 10$) then viscous fingering (VF) will *always* emerge at some length scale; (ii) especially in WW systems, then this VF may be almost “invisible” in lab-scale experiments where the WW P_c will wash out any viscous fingering as shown in our experiments (Fig. 17).

We note that a view often expressed in the porous media/reservoir engineering community is that: “*immiscible viscous fingering is really a lab-scale phenomenon, which probably does not occur in the field*”. This work indicates that the *opposite* is actually true; i.e. immiscible viscous fingering is actually quite difficult to see in the lab in a porous medium. However, if it does occur, then VF is *easier* to see in an OW (or neutral wet) system rather than in a WW system at the lab scale; more precisely in a system where $D(S_w) \approx 0$, especially in the region of the shock front at $S_w = S_{wf}$.

Non-equilibrium P_c and viscous fingering Finally, in all of the simulations presented here, we are using *equilibrium* P_c curves, i.e. assuming that the capillary pressure locally achieves its equilibrium value. There may be an effect of *non-equilibrium* P_c behaviour in viscous fingering. A large literature exists on *non-equilibrium* P_c in two-phase transport from Barenblatt et al. (2003); and many earlier references therein), to later development and the review in Aryan and Kovscek (2013). Our initial thoughts are that this would tend to *enhance* viscous fingering, particularly in WW systems. We believe that, using the methods developed in this work which give very well-developed fingering in the viscous-dominated case, non-equilibrium P_c effects on fingering can now be fruitfully explored.

7.3 Specific Conclusions of this Work

The detailed conclusions of this study are as follows:

Our previous work, and the additional results in this paper, shows that fully developed viscous fingering is now straightforward to produce for the *viscous-dominated* case ($P_c=0$; or scaling group $C_{VCI} \rightarrow \infty$) using direct numerical simulation by applying our recently proposed methodology (Sorbie et al. 2020). In reality, where there will be both viscous and capillary forces, viscous fingering can be observed experimentally at the lab scale (under certain conditions) and *always* (in our view) at the field scale, for values of $(\mu_o/\mu_w) > > 1$. Indeed, in the viscous-dominated limit, there is a direct scaling from the lab scale of a 2D experiment directly to the field scale, if the mixing length scales directly with system size; i.e. dispersivity, $\alpha \approx \delta x/2$, where the grid size, $\delta x = L/N$, where L is the (lab or field) size and N is the (same) number of grid blocks. This is demonstrated numerically in this paper.

Using our methodology to derive the viscous-dominated case and including water wet (WW) P_c in our simulations (Curve A P_c) shows that, at the experimental (lab) scale almost any level of WW P_c will significantly suppress clearly observable VF even in highly adverse viscosity ratios, such as in the $(\mu_o/\mu_w)=2000$ base case used in this work. Experimental results from a WW pack flood with $(\mu_o/\mu_w) \approx 100$ are presented to confirm this conclusion; viscous fingering is almost completely suppressed in this water \rightarrow oil displacement flood.

Following this second conclusion, the simulation results for the WW P_c case with a “high” P_c effect (Curve A P_c) were taken where the fingers were completely suppressed; this implies a finite and “low” value of the viscous/capillary scaling group, $C_{VCI} = \zeta$. This simulation case was then systematically rescaled by holding the P_c constant (i.e. dP_c/dS_w is constant in C_{VCI}) and the system size was increased. This changes the viscous/capillary force balance, represented by the scaling group, C_{VCI} (with a constant shape group C_{VCI}). It is demonstrated that as the system size increases, the effect of the P_c becomes less important ($C_{VCI} > \zeta$) and fully developed viscous fingering emerges at the larger scale (where $C_{VCI} \gg \zeta$). Indeed, for WW systems viscous-dominated viscous fingering is quite difficult to observe at the lab scale, but it nevertheless exists at the field scale. This probably explains why virtually no experimental results showing clear viscous fingering have been produced for a lab-scale strongly WW system.

Adverse viscosity ratio calculations have been carried out in oil wet (OW) systems (Curves B and C type P_c), in which we demonstrate that it is *much more* likely to observe viscous fingering than in the WW case. However, the fingering can still either appear or be suppressed at the laboratory scale in OW systems; see conditions in conclusion below. In the OW system, the P_c shows a region between S_{wi} and S_{wx} where $(dP_c/dS_w) \approx 0$ (and hence $D(S_w) \approx 0$), at which point there is a turnover point where P_c becomes < 0 , (i.e. $(dP_c/dS_w) < 0$ and hence $D(S_w) > 0$; Curves B and C). This is supported experimentally in this work by using the same bead pack as used for the WW displacement for $(\mu_o/\mu_w)=100$, but the pack was converted by silanisation to being OW. In this experiment clear viscous fingering is observed, in obvious contrast the WW case.

There are conditions for clear viscous fingering in the OW P_c lab case mentioned in the conclusion above, as follows: Viscous fingering in the OW case is most strongly enhanced if (i) in the region $S_{wi} \leq S_w \leq S_w$ then the P_c is *constant* (i.e. $(dP_c/dS_w) \approx 0$ and ideally $(dP_c/dS_w) = 0$, as in Curve C), and (ii) if the P_c turnover point at $S_w = S_{wx}$ is somewhat *above* the Buckley–Leverett front height (S_{wf}) of the original f_w^* used in the simulation; i.e. the condition $S_{wf} < S_{wx}$ favours fingering for the OW case. Likewise, the condition $S_{wf} > S_{wx}$ leads to finger suppression for the OW case. Around this point at $S_w = S_{wx}$ the simulated viscous fingering shows very considerable sensitivity to capillary pressure.

The generalisation of the above conditions for viscous fingering to occur at the lab (or any) scale for a system of *any* wettability WW or OW (mixed or neutral wet) is simply related to the value of $D(S_w)$ in the region of the BL shock front. If $D(S_w) \approx 0$ (or is very low) close to $S_w = S_{wf}$, then well-developed fingering will be observed, if not the fingering will be suppressed (somewhat or completely). For a given system, there is therefore a value of the viscous/capillary scaling group (C_{VCI}) which will determine if the fingers form for a given $(\mu_o/\mu_w) \gg 1$ case; if $C_{VCI} > \zeta_{crit}$, then fingers will form, but due to the nonlinearity of the system, this is not a single number for all systems. Thus, a simple “capillary number” (like the “Peclet number” used here) is not of particular use in this respect, as a predictor of when developed viscous fingering will be observed.

A practical corollary going *from* the observed fingering experiments *back to the wetting state* of the system, is as follows: From the above analysis, it is evident that *if* well-defined immiscible viscous fingering *is observed* in the lab, then the experimental system is almost certainly oil wet (OW) or very weakly wetting (close to neutral wet with $\cos \theta_{ow} \approx 0$), i.e. it will have a region above $S_w = S_{wi}$ to some value we denote as $S_w = S_{wx}$ where $(dP_c/dS_w) \approx 0$. The experiments presented by Skauge et al. (referenced herein) over the last decade and more showed very clear fingering in 2D slabs of size $\sim 30\text{cm} \times 30\text{cm}$. These were Bentheimer sandstone slabs which were conditioned (at $S_w = S_{wi}$) by viscous reservoir crude oils at slightly elevated temperature, which rendered the system OW (or very weakly wetted by either phase) in the definition of this work, and hence viscous fingering could be observed very readily. Thus, these unstable immiscible floods are indeed “viscous dominated” and hence show clear viscous fingering.

Open Access This article is licensed under a Creative Commons Attribution 4.0 International License, which permits use, sharing, adaptation, distribution and reproduction in any medium or format, as long as you give appropriate credit to the original author(s) and the source, provide a link to the Creative Commons licence, and indicate if changes were made. The images or other third party material in this article are included in the article's Creative Commons licence, unless indicated otherwise in a credit line to the material. If material is not included in the article's Creative Commons licence and your intended use is not permitted by statutory regulation or exceeds the permitted use, you will need to obtain permission directly from the copyright holder. To view a copy of this licence, visit <http://creativecommons.org/licenses/by/4.0/>.

References

- Alemán, M.A., Slattery, J.C.: A linear stability analysis for immiscible displacements. *Transp. Porous Media* **3**, 455–472 (1988). <https://doi.org/10.1007/BF00138611>
- Arya, A., Hewett, T.A., Larson, R.G., Lake, L.W.: Dispersion and reservoir heterogeneity. *SPE Res. Eng.* **3**(01), 139–148 (1988). <https://doi.org/10.2118/14364-pa>
- Aryana, S.A., Kovscek, A.R.: Nonequilibrium effects and multiphase flow in porous media. *Transp. Porous Media* **97**, 373–394 (2013). <https://doi.org/10.1007/s11242-013-0129-y>
- Adam, A., Pavlidis, B., Percival, J.R., Salinas, P., De Loubens, R., Pain, C.C., Muggeridge, A.H., Jackson, M.D.: Dynamic mesh adaptivity for immiscible viscous fingering. SPE-182636-MS, Presented at the SPE Reservoir Simulation Conference, Montgomery, Texas, USA (2017). <https://doi.org/10.2118/182636-MS>
- Aziz, K., Settari, A.: *Petroleum Reservoir Simulation*. Applied Science Publishers, London (1979). <https://doi.org/10.2118/9781613999646>
- Bakharev, F., Campoli, L., Enin, A., Matveenko, S., Petrova, Y., Tikhomirov, S., Yakovlev, A.: Numerical investigation of viscous fingering phenomenon for raw field data. *Transp. Porous Media* **132**(2), 443–464 (2020). <https://doi.org/10.1007/s11242-020-01400-5>
- Barenblatt, G.I., Patzek, T.W., Silin, D.B.: The mathematical model of nonequilibrium effects in water-oil displacement. *SPE J.* 409–416 (2003)
- Bear, J.: *Dynamics of fluids in porous media*. Dover Civ. Mech. Eng. (1989)

- Berg, S., Ott, H.: Stability of CO₂-brine immiscible displacement. *Int. J. Greenh. Gas Control* **11**, 188–203 (2012). <https://doi.org/10.1016/j.ijggc.2012.07.001>
- Beteta, A., Sorbie, K.S., Skauge, A.: Immiscible viscous fingering: the simulation of tertiary polymer displacements of viscous oils in 2D slab floods. *Polymers* **14**, 4159 (2022). <https://doi.org/10.3390/polym14194159>
- Beteta, A., Sorbie, K.S., McIver, K., Johnson, G., Gasimov, R., van Zeil, W.: The role of immiscible fingering on the mechanism of secondary and tertiary polymer flooding of viscous oil. *Transp. Porous Media* (2022). <https://doi.org/10.1007/s11242-022-01774-8>
- Beteta, A., Sorbie, K.S., Johnson, G.: Immiscible viscous fingering at the field scale: numerical simulation of the captain polymer flood. *Under Review (available as pre-print)* (2023)
- Blunt, M., Barker, J.W., Rubin, B., Mansfield, M., Culverwell, I.D., Christie, M.A.: Predictive theory for viscous fingering in compositional displacement. *SPE Res. Eng.* **9**(01), 73–80 (1994). <https://doi.org/10.2118/24129-PA>
- Bondino, I., Nguyen, R., Hamon, G., Ormehaug, P., Skauge, A., Jouenne, S.: Tertiary polymer flooding in extra-heavy oil: an investigation using 1D and 2D experiments, core scale simulation and pore-scale network models. Paper presented at the International Symposium of the Society of Core Analysts, Austin, Texas, USA (2011)
- Calderon, G., Surguchev, L., Skjaeveland, S.: Fingering mechanism in heterogeneous porous media: a review. Paper presented at the IEA Collaborative Project on Enhanced Oil Recovery, 28th Annual Workshop and Symposium, Copenhagen, Denmark (2007)
- Chaudhuri, A., Vishnudas, R.: A systematic numerical modeling study of various polymer injection conditions on immiscible and miscible viscous fingering and oil recovery in a five-spot setup. *Fuel* **232**, 431–443 (2018). <https://doi.org/10.1016/j.fuel.2018.05.115>
- Chikhliwala, E.D., Huang, A.B., Yortsos, Y.C.: Numerical study of the linear stability of immiscible displacements in porous media. *Transp. Porous Media* **3**, 257 (1988)
- Chouke, R.L., van Meurs, P., van der Poel, C.: The instability of slow, immiscible, viscous liquid-liquid displacements in permeable media. In: *Petroleum Transactions, AIME*, vol. 216, pp. 188–194 (1959)
- Daripa, P., Pasa, G.: On capillary slowdown of viscous fingering in immiscible displacement in porous media. *TIPM* (2008). <https://doi.org/10.1007/s11242-008-9211-2>
- De Loubens, R., Vaillant, G., Regaieg, M., Yang, J., Moncorge, A., Fabbri, C., Darche, G.: Numerical modeling of unstable waterfloods and tertiary polymer floods into high viscous oils. paper SPE 182638. *SPE J.* (2018)
- Dixit, A.B., McDougall, S.R., Sorbie, K.S., Buckley, J.S.: Pore-scale modeling of wettability effects and their influence on oil recovery. *SPE Reserv. Eval. Eng.* **2**(1) (1999)
- Dixit, A.B., Buckley, J.S., McDougall, S.R., Sorbie, K.S.: Empirical measures of wettability in porous media and the relationship between them derived from pore-scale modelling. *Transp. Porous Media* **40**, 27–54 (2000)
- Doorwar, S., Mohanty, K.K.: Viscous fingering during non-thermal heavy oil recovery. Presented at SPE Annual Technical Conference and Exhibition, Denver, Colorado, USA, SPE-146841-MS (2011). <https://doi.org/10.2118/146841-MS>
- Doorwar, S., Mohanty, K.K.: Extension of the dielectric breakdown model for simulation of viscous fingering at finite viscosity ratios. *Phys. Rev. E* **90**(1), 013028 (2014a)
- Doorwar, S., Mohanty, K.K.: Polymer flood of viscous oils in complex carbonates, SPE-169162-MS, SPE Improved Oil Recovery Symposium, Tulsa, Oklahoma, USA, 12–16 April (2014b)
- Doorwar, S., Mohanty, K.K.: Viscous fingering function for unstable immiscible flows. *SPE J.* (2017). <https://doi.org/10.2118/173290-MS>
- Doorwar, S., Ambastha, A.: Pseudorelative permeabilities for simulation of unstable viscous oil displacement. *SPE Res. Eng. Eval.* **25**, 1403–1419 (2020)
- Drazin, P.G., Reid, W.H.: *Hydrodynamic Stability*, 2nd edn. Cambridge University Press, Cambridge (2004)
- Engelberts, W.F., Klinkenberg, L.J.: Laboratory experiments on the displacement of oil by water from packs of granular material. Presented at 3rd World Petroleum Congress, 28 May-6 June, The Hague, the Netherlands, WPC-4138 (1951)
- Erandi, D.I., Wijeratne, N., Halvorsen, B.M.: Computational study of fingering phenomenon in heavy oil reservoir with water drive. *Fuel* **158**, 306–314 (2015)
- Fabbri, C., De Loubens, R., Skauge, A., Ormehaug, P., Vik, B., Bourgeois, M., Morel, D., Hamon, G.: Comparison of history-matched water flood, tertiary polymer flood relative permeability's and evidence of hysteresis during tertiary polymer flood in very viscous oils. Paper presented at the SPE Asia Pacific Enhanced Oil Recovery Conference (2015)

- Fabbri, C., De-Loubens, R., Skauge, A., Hamon, G., Bourgeois, M.: Effect of initial water flooding on the performance of polymer flooding for heavy oil production. *Oil Gas Sci. Technol. Revue d'IFP Energies Nouvelles* **75**, 19 (2020)
- Fayers, F.J.: An approximate model with physically interpretable parameters for representing miscible viscous fingering. *SPE Res. Eng.* (1988)
- Fayers, F.J., Newley, T.M.J.: Detailed validation of an empirical model for viscous fingering with gravity effects. *SPE Res. Eng.* **3**(2), 542–550 (1988). <https://doi.org/10.2118/15993-PA>
- Hamid, S.A., Muggeridge, A.: Viscous fingering in reservoirs with long aspect ratios. Presented at SPE Improved Oil Recovery Conference, Tulsa, Oklahoma, USA, SPE-190294-MS, 14–18 April (2018). <https://doi.org/10.2118/190294-MS>
- Hill, S.: Channelling in packed columns. *Chem. Eng. Sci.* **1**, 274–253 (1952)
- Holbrook, O.C., Bernard, G.G.: Determination of wettability by dye adsorption. *Trans. AIME* **213**, 261–264 (1958). <https://doi.org/10.2118/896-G>
- Homsy, G.M.: Viscous fingering in porous media. *Ann. Rev. Fluid Mech.* **19**(1), 271–311 (1987)
- Huang, A.B., Chikhliwala, E.D., Yortsos, Y.C.: Linear stability analysis of immiscible displacements including continuously changing mobility and capillary effects: Part II General basic profiles. SPE Paper 13163, 59th Annual SPE Meeting, Houston, TX (1984)
- Kampitsis, A., Salinas, P., Pain, C., Muggeridge, A., Jackson, M.: Mesh adaptivity and parallel computing for 3D simulation of immiscible viscous fingering. Paper presented at the 20th European Symposium on Improved Oil Recovery (2019)
- Kampitsis, A.E., Adam, A., Salinas, P., Pain, C.C., Muggeridge, A.H., Jackson, M.D.: Dynamic adaptive mesh optimisation for immiscible viscous fingering. *Comput. Geosci.* (2020). <https://doi.org/10.1007/s10596-020-09938-5>
- Koval, E.J.: A Method for predicting the performance of unstable miscible displacement in heterogeneous media. *SPEJ* **2**(2), 145–154 (1963). <https://doi.org/10.2118/450-PA>
- Leverett, M.C.: Capillary behaviour in porous solids. *Trans. AIME* **142**, 159–172 (1941)
- Lomeland, F., Ebeltoft, E., Thomas, W.H.: A new versatile relative permeability correlation. Paper presented at the International symposium of the society of Core Analysts, Toronto, Canada (2005)
- Maini, B., Koskuner, G., Jha, K.A.: Comparison of steady-state and unsteady-state relative permeabilities of viscous oil and water in Ottawa sand. *J. Can. Pet. Technol* **29**(02) (1990)
- Maini, B.: It is futile to measure relative permeabilities for heavy oil reservoirs? *J. Can. Pet. Technol* **37**(04) (1998)
- Mostaghimi, P., Kamali, F., Jackson, M.D., Muggeridge, A.H., Paon, C.C.: Adaptive mesh optimization for simulation of immiscible viscous fingering, Paper SPE-173281-PA. *SPE J.* **21**(06), 2250–2259 (2016). <https://doi.org/10.2118/173281-PA>
- Peaceman, D.W.: Fundamentals of numerical reservoir simulation. In: *Developments in Petroleum Science*, vol. 6. Elsevier (1977)
- Rapoport, L.A.: Scaling laws for use in design and operation of water oil flow models. *Pet. Trans. AIME* **204**, 143–150 (1955)
- Pinder, G.F., Gray, W.G.: *Essentials of Multiphase Transport in Porous Media*. Wiley, New York (2008). <https://doi.org/10.1002/9780470380802>
- Pinilla, A., Asuaje, M., Ratkovich, N.: Experimental and computational advances on the study of viscous fingering: an umbrella review. *Heliyon J.* **7**, 25 (2021)
- Riaz, A., Tchelepi, H.A.: Numerical simulation of immiscible two phase flow in porous media. *Phys. Fluids* **18**, 014104 (2006a). <https://doi.org/10.1063/1.2166388>
- Riaz, A., Tchelepi, H.A.: Influence of relative permeability on the stability characteristics of immiscible flow in porous media. *Transp. Porous Media* **64**, 315–338 (2006b). <https://doi.org/10.1007/s11242-005-4312-7>
- Ryazanov, A.V., van Dijke, M.I.J., Sorbie, K.S.: Two-phase pore-network modelling: existence of oil layers during water invasion. *Transp. Porous Media* **80**, 79–99 (2009)
- Saffman, P.G., Taylor, G.I.: The penetration of a fluid into a porous medium or Hele-Shaw cell containing a more viscous liquid. *Proc. r. Soc. Lond. Ser. A* **245**, 312–329 (1958)
- Salmo, I.C., Pettersen, Ø., Skauge, A.: Polymer flooding at an adverse mobility ratio: acceleration of oil production by crossflow into water channels. *Energy Fuels* **31**(6), 5948–5958 (2017)
- Salmo, I.C., Sorbie, K.S., Skauge, A., Alzaabi, M.A.: Immiscible viscous fingering: modelling unstable water-oil displacement experiments in porous media. *Transp. Porous Media* **145**, 291–322 (2022). <https://doi.org/10.1007/s11242-022-01847-8>
- Skauge, A., Sorbie, K.S., Ormehaug, P.A., Skauge, T.: Experimental and numerical modeling studies of viscous unstable displacement. Paper presented at the IOR 2009-15th European Symposium on Improved Oil Recovery (2009)

- Skauge, A., Horgen, T., Noremark, B., Vik, B.: Experimental studies of unstable displacement in carbonate and sandstone material. Paper presented at the IOR 2011-16th European Symposium on Improved Oil Recovery (2011)
- Skauge, A., Ormehaug, P.A., Gurholt, T., Vik, B., Bondino, I., Hamon, G.: 2-D visualisation of unstable waterflood and polymer flood for displacement of heavy oil. Paper presented at the SPE Improved Oil Recovery Symposium (2012)
- Skauge, A., Ormehaug, P.A., Vik, B., Fabbri, C., Bondino, I., Hamon, G.: Polymer flood design for displacement of heavy oil analysed by 2D-imaging. Paper presented at the IOR 2013-17th European Symposium on Improved Oil Recovery (2013)
- Skauge, T., Vik, B.F., Ormehaug, P.A., Jatten, B.K., Kippe, V., Skjevraak, I., Standnes, D.C., Uleberg, K., Skauge, A.: Polymer flood at adverse mobility ratio in 2D flow by x-ray visualization. Paper presented at the SPE EOR Conference at Oil and Gas West Asia (2014)
- Skauge, A., Salmo, I.C.: Relative permeability functions for tertiary polymer flooding. Paper presented at the IOR 2015-18th European Symposium on Improved Oil Recovery (2015)
- Sorbie, K.S., Al Ghafri, A., Skauge, A., Mackay, E.: On the modelling of immiscible viscous fingering in two-phase flow in porous media. *Transp. Porous Media* **135**(2), 331–359 (2020)
- Sorbie, K.S.: Presentation: Scaling Theory for Two Phase Flow in Porous Media (after Rapoport, 1955); additional material which extends and clarified Rapoport's paper—supplied in the downloadable supplementary material with this paper (2023)
- Stephen, K.D., Pickup, G.E., Sorbie, K.S.: The local analysis of changing force balances in immiscible, incompressible two-phase flow. *Transp. Porous Media* **45**(1), 63–88 (2001)
- Tardy, P.J.M., Pearson, J.R.A.: A 1D-averaged model for stable and unstable miscible flows in porous media with varying Peclet numbers and aspect ratios. *Transp. Porous Media* **62**, 205–232 (2006)
- Van Meurs, P., Van der Poel, C.: A theoretical description of water-drive processes involving viscous fingering. *Trans. AIME* **213**(01), 103–112 (1958)
- Worawutthichanyakul, T., Mohanty, K.K.: Unstable immiscible displacements in oil-wet rocks. *Transp. Porous Media* **119**, 205–223 (2017). <https://doi.org/10.1007/s11242-017-0880-6>
- Wu, Y.-S.: *Multiphase Fluid Flow in Porous and Fractured Reservoirs*. Elsevier, New York (2015)
- Yortsos, Y.C., Hickernell, F.J.: Linear stability of immiscible displacement in porous media. *SIAM (soc. Ind. Appl. Math.) J. Appl. Math.* **49**, 730 (1989)
- Yortsos Y.C., Huang, A.B.: Linear stability an of immiscible displacement: Part 1—simple basic flow properties. *SPE Res. Eng.* 378–390 (1986)
- Yortsos, Y.C.: Instabilities in displacement processes in porous media. *J. Phys.: Condens. Matter* **2**, SA443 (1990)
- Zhao, B.: Effect of Wettability on Viscous Fingering During Unstable Immiscible Displacement. Ph.D. Dissertation, The University of Texas at Austin (2020)
- Zhao, B., Mohanty, K.K.: Effect of wettability on immiscible viscous fingering in porous media. *J. Petrol. Sci. Eng.* **174**, 738–746 (2019)
- Zhou, X., Morrow, N.R., Ma, S.: Interrelationship of wettability, initial water saturation, aging time, and oil recovery by spontaneous imbibition and waterflooding. *SPE J.* **5**(02), 199–207 (2000). <https://doi.org/10.2118/62507-PA>

Publisher's Note Springer Nature remains neutral with regard to jurisdictional claims in published maps and institutional affiliations.

Authors and Affiliations

A. Beteta¹ · K. S. Sorbie^{1,2}  · A. Skauge^{1,2} · T. Skauge²

✉ K. S. Sorbie
k.sorbie@hw.ac.uk

¹ Institute of GeoEnergy Engineering (IGE), Heriot-Watt University, Edinburgh, UK

² Energy Research Norway (ERN), Bergen, Norway